

## Article

# The Lanthanide “Tetrad Effect” as an Exploration Tool for Granite-Related Rare Metal Ore Systems: Examples from the Iberian Variscan Belt

Ivo Martins <sup>1,2,\*</sup> , António Mateus <sup>1,2</sup> , Michel Cathelineau <sup>3</sup> , Marie Christine Boiron <sup>3</sup> , Isabel Ribeiro da Costa <sup>1</sup> , Ícaro Dias da Silva <sup>1,2</sup>  and Miguel Gaspar <sup>1</sup> 

<sup>1</sup> Departamento de Geologia, Faculdade de Ciências da Universidade de Lisboa, Ed. C6, Piso 4, Campo Grande, 1749-016 Lisboa, Portugal

<sup>2</sup> Instituto Dom Luiz (IDL), Faculdade de Ciências da Universidade de Lisboa, Ed. C1, Piso 1, Campo Grande, 1749-016 Lisboa, Portugal

<sup>3</sup> Université de Lorraine, CNRS, GeoRessources, F-54000 Nancy, France

\* Correspondence: [ijmartins@fc.ul.pt](mailto:ijmartins@fc.ul.pt)

**Abstract:** Highly fractionated granites and related magmatic-hydrothermal ore-forming processes can be traced by elemental ratios such as Nb/Ta, K/Rb, Y/Ho, Sr/Eu, Eu/Eu\*, Zr/Hf, and Rb/Sr. The lanthanide “tetrad effect” parameter ( $TE_{1,3}$ ) can also be a useful geochemical fingerprint of highly fractionated granites. This work assesses its application as an exploration vector for granite-related mineralization in the Central Iberian Zone by examining  $TE_{1,3}$  variations with different elemental ratios and with the concentrations of rare metals and fluxing elements (such as F, P, and B). The multi-elemental whole-rock characterization of the main Cambrian–Ordovician and Carboniferous–Permian granite plutons and late aplite–pegmatite dykes exposed across the Segura–Panasqueira Sn-W-Li belt show that the increase in  $TE_{1,3}$  values co-vary with magmatic differentiation and metal-enrichment, being the Carboniferous–Permian granite rocks the most differentiated, and metal specialized. The Argemela Li-Sn-bearing rare metal granite and the Segura Li-phosphate-bearing aplite–pegmatite dykes deviate from this geochemical trend, displaying  $TE_{1,3} < 1.1$ , but high  $P_2O_5$  contents. The results suggest that mineralized rocks related to peraluminous-high-phosphorus Li-Sn granite systems are typified by  $TE_{1,3} < 1.1$ , whereas those associated with peraluminous-high-phosphorus Sn-W-Li (lepidolite) and peraluminous-low-phosphorus Sn-Ta-Nb granite systems display  $TE_{1,3} > 1.1$ , reaching values as high as 1.4 and 2.1, respectively.

**Keywords:** CIZ magmatism; granite differentiation; granite-related ore systems; lanthanide tetrad effect; mineral exploration



**Citation:** Martins, I.; Mateus, A.; Cathelineau, M.; Boiron, M.C.; Ribeiro da Costa, I.; Dias da Silva, Í.; Gaspar, M. The Lanthanide “Tetrad Effect” as an Exploration Tool for Granite-Related Rare Metal Ore Systems: Examples from the Iberian Variscan Belt. *Minerals* **2022**, *12*, 1067. <https://doi.org/10.3390/min12091067>

Academic Editor: Panagiotis Voudouris

Received: 28 July 2022

Accepted: 22 August 2022

Published: 24 August 2022

**Publisher’s Note:** MDPI stays neutral with regard to jurisdictional claims in published maps and institutional affiliations.



**Copyright:** © 2022 by the authors. Licensee MDPI, Basel, Switzerland. This article is an open access article distributed under the terms and conditions of the Creative Commons Attribution (CC BY) license (<https://creativecommons.org/licenses/by/4.0/>).

## 1. Introduction

Current technological development and energy transition policies amplify our dependence on a large number of metals with low recycling rates. Such context generates additional pressure on mineral exploration endeavors to search for new primary resources of these strategic metals, which are often associated with highly evolved muscovite-bearing peraluminous granites [1–4].

Granite-related ore systems include mainly: (i) quartz lodes, breccia pipes and skarns enriched in W-Sn-F(-P)-bearing mineral assemblages, and (ii) rare-metal granites and pegmatite-hosted mineral assemblages enriched in Li-Cs-Be-Ta(-P) and Nb-Y-F(-Sn) (e.g., [1,5,6]). Numerous granite-related ore systems with different mineralization styles coexist in Europe, forming a world-class Sn-W-Li province of Paleozoic age [7–15]. The Segura–Panasqueira area, in the Central Iberian Zone (CIZ—the central geotectonic unit of the Iberian Variscan belt), is part of the well-defined Late Palaeozoic granite-related European metallogenic belt, where voluminous peraluminous granite suites with distinct degrees of differentiation are associated with varied W, Sn, and Li ore systems.

Highly fractionated granites and associated magmatic-hydrothermal ore-forming processes can be traced by elemental content ratios such as K/Rb, Sr/Eu, Y/Ho, Rb/Sr, Nb/Ta, and Zr/Hf [4,16–20]. The lanthanide tetrad effect has also been used as a geochemical marker of magmatic evolution and magmatic-hydrothermal transition, corresponding to a specific form of rare earth element (REE) fractionation, evidenced by the subdivision of the chondrite-normalized REE patterns into four curved segments that are called tetrads [18,21]. There are two types of REE patterns portraying the tetrad effect, with the curved segments being either convex (M-type) or concave (W-type) [16–18]. This REE fractionation is commonly observed in highly evolved felsic magmatic rocks and related metasomatic rocks, as well as in mineral precipitates from hydrothermal fluids, accessory minerals and melt inclusions [16,18,22–27]. The M-type pattern may represent highly evolved granites from which a coexisting fluid, with a W-type REE pattern, is extracted [18,21,28,29]. Yet, other studies [30,31] indicate that conventional magmatic crystallization alone can yield similar M-type patterns and melt-fluid immiscibility is not needed to explain tetrad-like REE patterns. Nevertheless, deviation of the tetrad curved segments from a theoretical “tetrad effect”-free chondrite-normalized REE pattern can be quantified, such as the degree of tetrad effect ( $TE_{1,3}$ —deviation of the first and third tetrad) which is considered significant when  $TE_{1,3} > 1.1$  [18].

In this work, the application of the  $TE_{1,3}$  as an exploration vector for granite-related mineralization is assessed by examining the  $TE_{1,3}$  variations along with other geochemical parameters and the contents of rare metals (Sn, W, Nb, Ta, and Li) and fluxing elements. New whole-rock multi-elemental geochemical data of the main (composite) plutons and dykes exposed across the Segura–Panasqueira area are reported, supporting a comprehensive geochemical characterization of: (i) granite and granodiorite rocks that represent different regional magmatic pulses; and (ii) late Rare Metal Granite (RMG), aplite–pegmatite dykes, and greisen rocks from Argemela, Segura, and Panasqueira representing the W, Sn, and Li granite-related ore systems. The degree of differentiation and mineralization potential, as well as the applicability of the  $TE_{1,3}$  as an exploration tool for granite-related ore systems are discussed, along with the geochemical composition of granite rocks from other sectors of the Variscan belt.

## 2. Geological Setting

The Segura–Panasqueira area is located in the CIZ, which forms the central part of the Iberian segment of the Variscan orogenic belt (Figure 1a). The Gondwana–Laurussia collision and subsequent closure of the Rheic Ocean (Middle-Devonian to Middle-Upper Mississippian), followed by late (post-thickening) lithospheric rebound and stress relieving (Middle-Upper Mississippian to Permian), have primarily controlled the tectonic evolution of the Variscan belt [32–36].

Three main deformation phases (D1, D2 and D3) have been distinguished in this domain of the Variscan orogenic belt [32,33,37–41]. The D1 and D2 deformation phases (359–336 and 337–316 Ma, respectively) [35,42–44] reflect the maximum Variscan crustal shortening during which folds of large amplitude were generated: these folds display variable geometry and orientation depending on the orogenic sector, presenting an NW-SE preferred strike with sub-vertical axial planes [33,45].

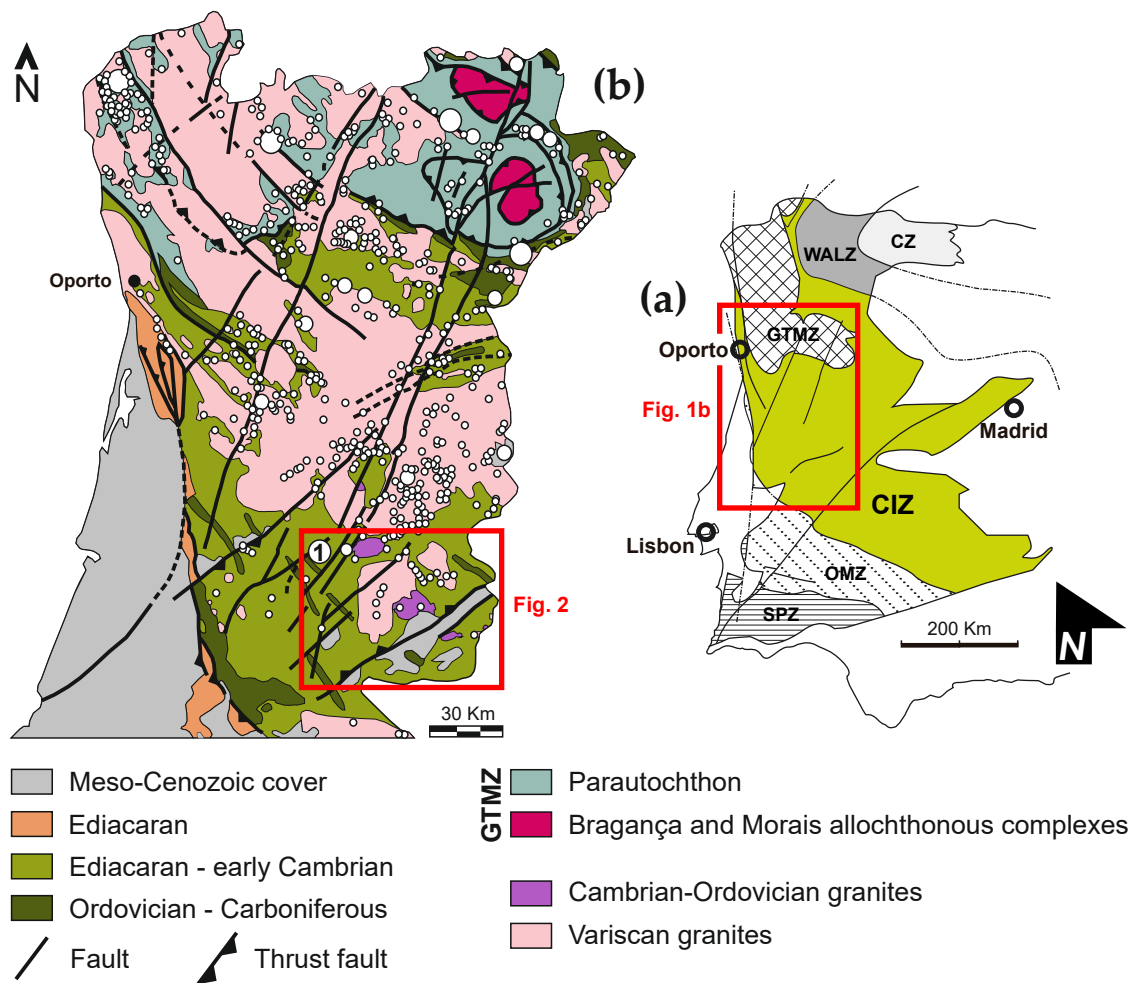


**Figure 1.** (a) Geotectonic map of the Iberian Massif (adapted from [46,47]). CZ—Cantabrian Zone; WALZ—West Asturian-Leonese Zone; GTMZ—alicia Trás-os-Montes Zone; CIZ—Central Iberian Zone; OMZ—Ossa Morena Zone; SPZ—South Portuguese Zone. (b) Simplified geological map of central and northern Portugal (adapted from “Carta Geológica de Portugal 1:1,000,000”, Geological Survey of Portugal, LNEG, 2010; modified from [48]). White circles represent the main known tungsten and tin deposits (mineral deposits location taken from the official national catalog SIORMINP-LNEG). 1—Panasqueira Mine.

Concurrently with D1 folding and often reflecting thermo-mechanic contrasts generated during heterogeneous strain accommodation, several regional ductile syn-D1 shear zones were also developed. After tectonic emplacement of the allochthonous piles typifying NW Iberia and the HT-LP event affecting the underlying CIZ (D2-M2, after [41,47]), intra-continental strike-slip sinistral and dextral sub-vertical semi-brittle shear zones were formed during D3 [49–54], together with folds displaying sub-vertical axial plane and sub-horizontal axis [45,50–55]. These sub-vertical shear zones, locally reactivating previous syn-D1 shears, are often confined to the edges of voluminous granite batholiths [38,56–62]. Spatial distribution of shear zones and folds indicates NE-SW maximum compression trajectories [63], not deviating significantly from the stress configuration characterizing the previous deformation phases. The D3 (315–306 Ma) [39,44,56] deformation phase took place mostly after the climax of crustal thickening, followed by decompression and HT-LP metamorphism during which large volumes of crustal melting were produced [39,55,64–68]. Late- to post-D3 (300–270 Ma) [63,69], conjugate strike-slip fault systems running NNE-SSW (left-lateral) and NNW-SSE (right-lateral) were further generated in brittle conditions, locally reactivating syn-D3 (and syn-D1) shear zones (e.g., [37–39,45]).

The Beira–Baixa region, which includes the Segura–Panasqueira area, comprises voluminous granite bodies hosted in a folded siliciclastic metasedimentary sequence that was recrystallized under greenschist P–T conditions of greenschist metamorphic facies. The metasedimentary sequence corresponds to the Dúrico–Beirão Supergroup (e.g., [70–74]), which includes the Douro Group (Cambrian Stage 1 to Stage 4) and the Beiras Group (Ediacaran to Cambrian Stage 3, “Marianian–Bilbilian”) [75–77]. Granitoid rocks cropping out in the CIZ show a wide range of facies and compositions [40], resulting from partial melting of various protoliths, at the mid–lower crust transition, such as metapelites, meta-greywackes, and metavolcanic rocks. In some cases, contributions from lower crustal granulites were also proposed (e.g., [56,78–80]). Following criteria based on the age relationship between the emplacement of these rocks and the D3 phase, these granites are usually classified into four main subgroups (e.g., [56,81–84]):

- (i) Syn-D3 (ca. 320 to 310 Ma)—two-mica granites, strongly peraluminous, with aluminum-potassic affinity, representing magmas derived from partial melting of metapelites;
- (ii) Late-D3 (ca. 310 to 305 Ma)—moderately peraluminous and aluminum-potassium biotitic monzogranites/granodiorites with aluminum-potassic affinity, resulting from crystallization of magmas generated from partial melting of metagreywacke and felsic meta-igneous materials;
- (iii) Late- to post-D3 (ca. 300 Ma)—peraluminous two-mica leucogranite with high aluminum-potassic affinity;
- (iv) Post-D3 (ca. 296 to 290 Ma)—compositionally evolved granitoids with an iron-potassic sub-alkaline affinity as products from the partial melting of lower crustal rocks.

The geological evolution of Iberia during Paleozoic times conditioned the spatial distribution of granitic bodies along specific crustal alignments in the CIZ (e.g., [45,56]). The generation of the prevalent melts was roughly contemporary of the D3 folding, favoring granite emplacement across the core of major D3 anticlines (e.g., [40]). Thermo-mechanical contrasts developed during cooling of these granites and their country rocks, under a strong stress regime, led to nucleation and propagation of syn-D3 shear zones, further representing the preferred loci for strain accommodation. Locally, these tectonic discontinuities played an essential role as conduits of melts generated and emplaced in late-, late- to post-, and post-D3 times (e.g., [45]). The relative intensity of the regional stress field and local interferences with stress fields related to the emplacement/cooling of granite bodies prompted the development of several subsidiary structures which may have reactivated pre-existing mechanical discontinuities in country rocks (e.g., [85–88]).

The known epigenetic mineralized systems in the CIZ are closely related to the granite suites mentioned above, at least spatially (Figure 1b). This highlights the importance/influence of the Variscan orogeny in the onset and development of different metallogenic processes over millions of years, leading to the formation of distinct but spatially coexistent ore systems (e.g., [84]). The spatial distribution of Sn, W, and Li occurrences follows the dispersion of outcropping or sub-superficial granite bodies, the latter often evidenced by contact metamorphic aureoles of variable extension and distinct mineral associations. Although clear spatial relationships between granite suites and ore deposits, the Sn, W, and Li mineralizing systems are not exclusively related to magmatic activity as these ore-forming processes are multiphase and long-lived, including the late magmatic stages but also fluid convection around heat spots (e.g., [14,48,84,89]). Therefore, the granite–metasedimentary binary is relevant not only in generating some melts but also to the constraints imposed on the production of hydrothermal fluids (volume and composition) involved in the ore-forming processes (e.g., [90]).

The location of the main W, Sn, and Li ore systems is largely controlled by inherited structures (such as shear zones and other structural lithospheric weakness zones) that were also determinant for the emplacement of post-tectonic granites [91], both occurring along granite–metasediment or diachronic granite contacts [92]. The mineralization centers may arise in endo- and exo-contact domains, contributing to the development of geochemical zoning patterns often described by the following sequence: Sn–Li-bearing pegmatites and

Sn-Li-bearing quartz veins within endo-contact domains; Sn-W quartz veins scattered over the endo/exo-contact transition, but extending preferentially to exo-contact fields; and W-quartz veins within the exo-contact environments [93].

The Segura–Panasqueira area, the focus of this study, is characterized by a siliciclastic (shale-greywacke) metasedimentary sequence belonging to the Beiras Group hosting several voluminous granite bodies. Numerous mineral occurrences were recognized in this area, indicating significant metallogenic potential (Figure 1b). Three main groups of granitoid rocks are known in the Segura–Panasqueira area (Figure 2), which document two (relatively short) events of magmatic activity favorable to the generation and emplacement of felsic magmas [94–104]. The first group includes (i) two mica granitoids with metasedimentary restites, (ii) biotite quartz-diorites and granodiorites, and (iii) non-porphyroid granites and granodiorites, representing a Cambrian–Ordovician magmatic event spreading for about 20 Ma (from ca. 490 Ma to 470 Ma). The two remaining groups, syn- to late-D3 and late- to post-D3, represent a Carboniferous–Permian (late- to post-Variscan) magmatic event which lasted for approximately 30 Ma (from ca. 320 Ma to 290 Ma). The syn-D3 group comprises (i) porphyroid granites and granodiorites and (ii) undifferentiated two-mica granites. The late- to post-D3 group includes (i) two-mica granites, (ii) monzonitic granites with sparse feldspar megacrysts, (iii) porphyroid monzonitic granites, and (iv) usually porphyroid biotite granites. The last group also includes the highly differentiated granite rocks that are key references for granite-related ore systems, such as the Panasqueira granite, the Li-Sn Argemela RMG and the Li-Sn-bearing aplite–pegmatites dykes of Segura.

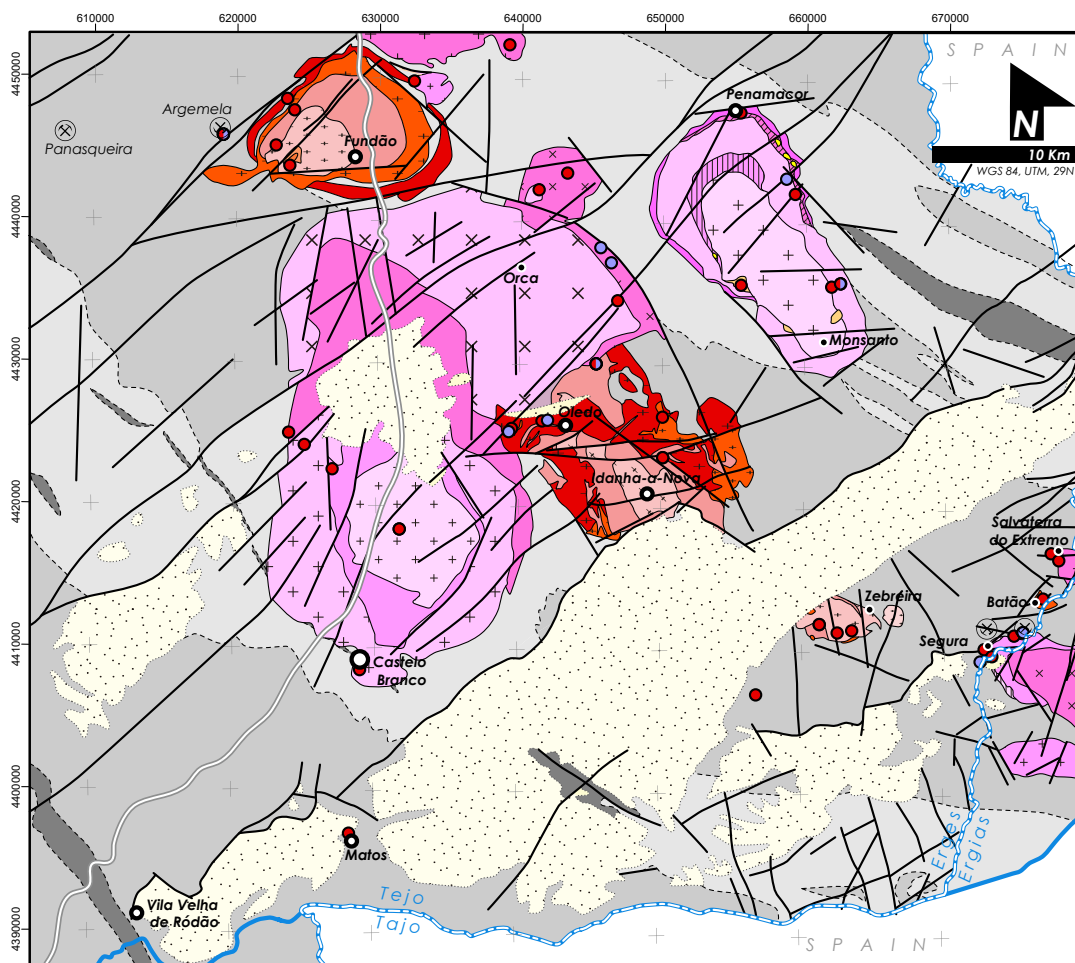
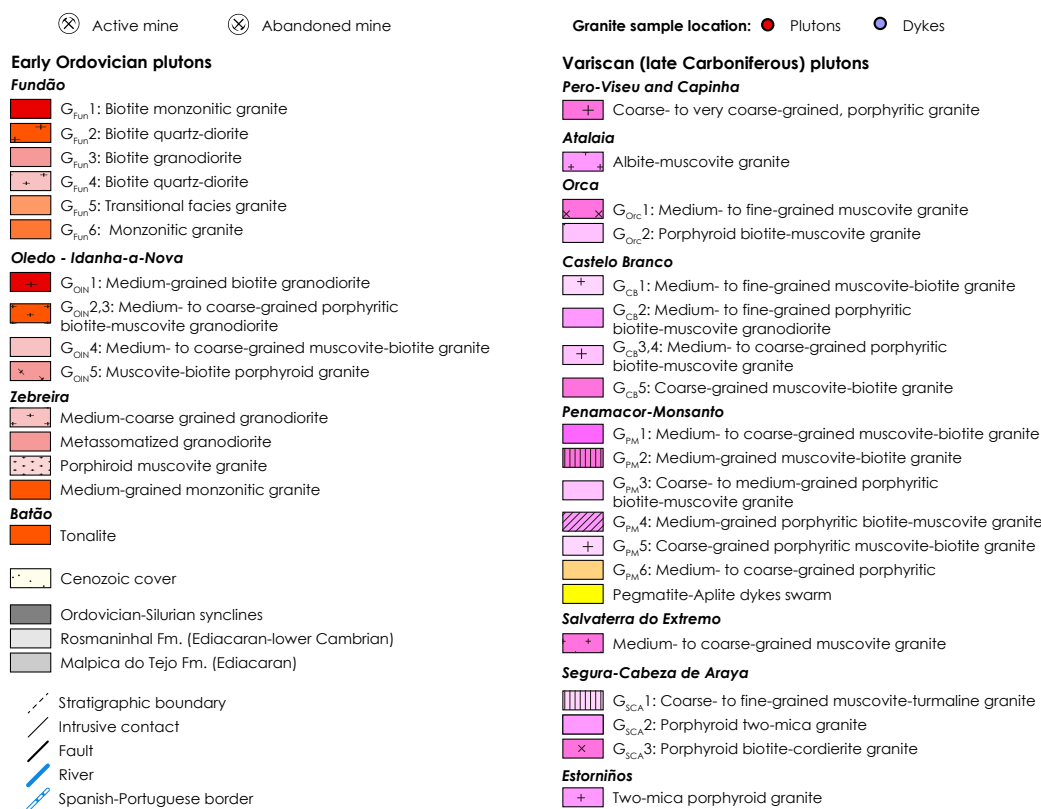


Figure 2. Cont.



**Figure 2.** Simplified geological map of the Segura–Panasqueira area with the sampling location. The map integrates recent field appraisals along with outputs from previous databases [74,105–112].

### 3. Sampling and Analytical Methods

In the 2019–2021 period, 197 representative samples of the different granite suites and highly differentiated granitic pegmatite and aplite veins exposed in the Segura–Panasqueira area were collected for multi-element whole-rock geochemical characterization (Figure 2). Sampling criteria were: (i) to complement existing data for exposed rock types by collecting granite facies from sites where information gaps existed; (ii) to achieve a spatially representative sampling of different outcropping igneous facies; (iii) to sample, preferentially, along waterlines and non-vegetated river margins where the bedrock is usually better preserved; (iv) to gather samples from different mineralization types, to identify geochemical fingerprints imposed by hydrothermal processes.

A total of 75 samples were collected: (i) 51 samples of felsic igneous bodies; (ii) 18 samples of felsic igneous dykes; and (iii) 6 samples of greisen and episyenite rocks from the Panasqueira Mine area. Although most of the samples were collected from outcrops (58), critical drillings and mining works from Panasqueira and Argemela were also sampled (17). Key samples representing different granite facies (poorly to highly differentiated) were selected, processed, and sent to internationally accredited laboratories for high-precision whole-rock geochemical analysis (49). Whole-rock major and trace element concentrations were obtained at Activation Laboratories, Ltd. (Ancaster, ON, Canada), using the 4E-research-ICP-MS analytical package. Major oxide elements were analyzed by inductively coupled plasma optical emission spectrometry (ICP-OES). Trace and rare earth elements (REE) were obtained by induced coupled plasma mass spectrometry (ICP-MS) and instrumental neutron activation analysis (INAA). In addition, F, B, and FeO contents were measured by KOH-ion chromatography, Prompt gamma neutron activation analysis (PGNAA), and titration, respectively.

Detailed information regarding the analytical and control procedures is available in the Actlabs website ([www.actlabs.com](http://www.actlabs.com) (accessed on 21 August 2022)).

Afterwards, these samples were used as in-house standards for the remaining samples analyzed with X-ray fluorescence (XRF) at the Faculdade de Ciências da Universidade de Lisboa (Lisbon, Portugal). This analytical work used a wavelength dispersive Zetium XRF spectrometer (Malvern PANalytical) having a 4000 W “Super Sharp X-ray Tube” with rhodium anode and a CHI-BLUE window coating for superior light element performance. The apparatus also has a duplex xenon detector and a scintillation detector for elements heavier than Zn, as well as two flow (argon/methane) detectors for light and heavy elements. The installed crystals are LiF 200, LiF 220, Ge 111, PE 002, and PX-1. The SuperQ analytical software assisted all the measurements: the Omnia calibration for standardless analysis and ProTrace calibration for quantitative trace element analysis. Calibration for fully quantitative analysis of silicate-based materials were based on certified international standards. The accuracy-related errors in XRF measurements were  $\leq 5\%$  for major elements and better than 10% for the most incompatible elements. Duplicate measurements of samples indicate that reproducibility-related errors in XRF analyses were generally  $\leq 5\%$  for both major and trace elements.

#### 4. Results

The whole-rock multi-element data of the main (composite) granite plutons and aplite–pegmatite dykes exposed across the Segura–Panasqueira area are listed in Table S1. Facies description, previous geochronological information (Table S1), and field relationships indicate that the sampled rocks represent two main regional magmatic pulses: Cambrian–Ordovician and Carboniferous–Permian (Variscan). The Cambrian–Ordovician magmatic event is represented by the composite plutons of Zebreira [99], Oledo-Idanha-a-Nova [101], Fundão [102,104], Batão and Matos. The Variscan magmatic event is characterized by the Salvaterra do Extremo (Syn-D3?), Castelo Branco (Late-D3; [100]), Segura (Late-D3; [103]), Orca (Late-D3; [113]), Penamacor–Monsanto (Late- to Post-D3; [114,115]), Capinha (Late- to Post-D3; [113]), and Atalaia (Late- to Post-D3; [113]) plutons and a porphyry intrusion near Zebreira (Late- to Post-D3?). It is worth noting that in all the cross-plots, the intersection between the compositional fields of the two magmatic events is mainly due to the widespread distribution of samples representing the less differentiated facies of the Castelo Branco pluton (CB-G2) and the more differentiated facies of the Zebreira, Oledo-Idanha-a-Nova and Fundão plutons (G\_ZEB#1 and G\_ZEB#4; OIN-G3 and G4; FUN-G1 and FUN-G3). In addition, field observations suggest that these differentiated Cambrian–Ordovician facies are younger than the less evolved ones, often showing crisscrossing relationships and textural fabric contrasts that point to significant differences in their emplacement timing. Therefore, to clarify whether they are being attributed to the correct magmatic event or correspond to late magmatic pulses of Variscan age, these differentiated facies have been selected for future U–Pb zircon dating.

For purposes of geochemical interpretation, the aplite–pegmatite dykes from Oledo-Idanha-a-Nova, Orca, and Penamacor–Monsanto, together with granite rocks related to Li–Sn and W–Sn ore systems from Argemela [116], Segura, and Panasqueira [117], have been examined separately. As these rocks are highly differentiated and have interacted with magmatic–hydrothermal processes, they should not be used in conventional diagrams of geochemical classification of granitic rocks. As refers to the rare earth elements, only analyses with the lowest detection limits and complete REE patterns were considered. The degree of the tetrad effect was estimated by the methods of quantification proposed by Irber (1999) [18] and Monecke (2002) [28] (Tables S2 and S3). As both methods have yielded similar results, those of the  $TE_{1,3}$  [18] are presented in this work, for graphic simplicity.

##### 4.1. Major and Minor Elements

Most Cambrian–Ordovician granitoid rocks are weakly peraluminous I-type (average ASI value of 1.11), tonalite to granodiorite rocks (Figure 3). They present relatively moderate  $SiO_2$  contents (average value 68.2 wt. %), total alkalis (average  $Na_2O + K_2O$  value 6.87 wt. %) and  $FeO_{total}/(FeO_{total} + MgO)$  ratios (average  $Fe^*$  value 0.66), with most

samples plotting into the compositional fields of calcic to calc-alkalic series and magnesian granites (Figure 4a,b). In turn, Variscan magmatism is represented by highly peraluminous S-type (median ASI value 1.25), monzogranite to granite rocks (Figure 3). Variscan granite rocks show relatively high SiO<sub>2</sub> median content (72.7 wt. %), total alkalis (median value of 8.12 wt. %), and FeO<sub>total</sub>/(FeO<sub>total</sub> + MgO) ratios (median content 0.79), plotting into the compositional fields of calc-alkalic to alkali-calcic series and magnesian to ferroan granites (Figure 4a,b). Regarding their degree of differentiation, the Cambrian–Ordovician granitoid suites range from diorite to normal granite compositions and display condensed differentiation trends in comparison with those typical of Variscan granites. The latter are strongly differentiated rocks, as confirmed by their contents in Ba, Rb, and Sr (Figure 4c). Most of the Cambrian–Ordovician granitoid rocks plot in the compositional field of volcanic arc granites, whereas the Variscan granites cluster in the field of syn-collisional granites (Figure 5).

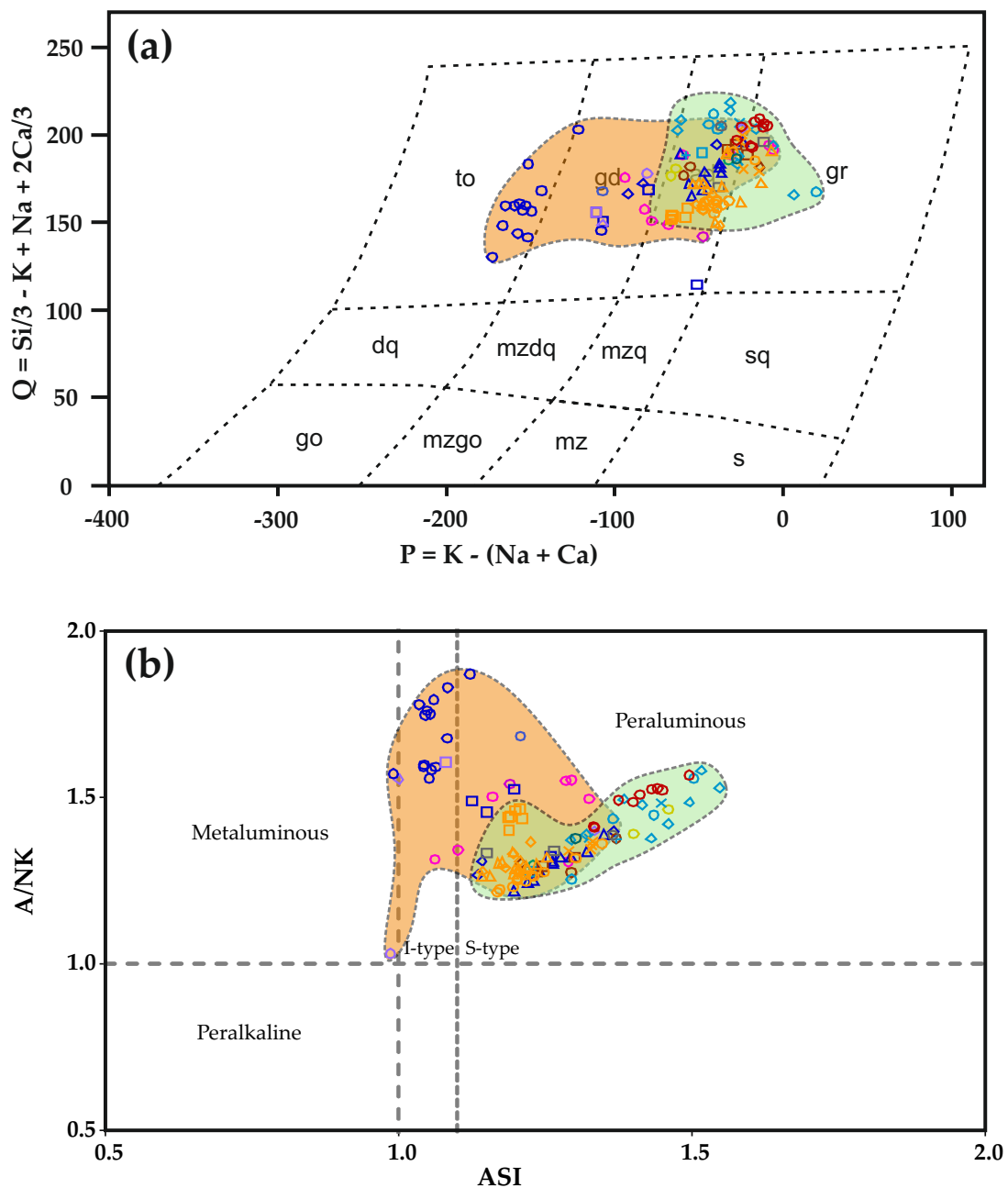
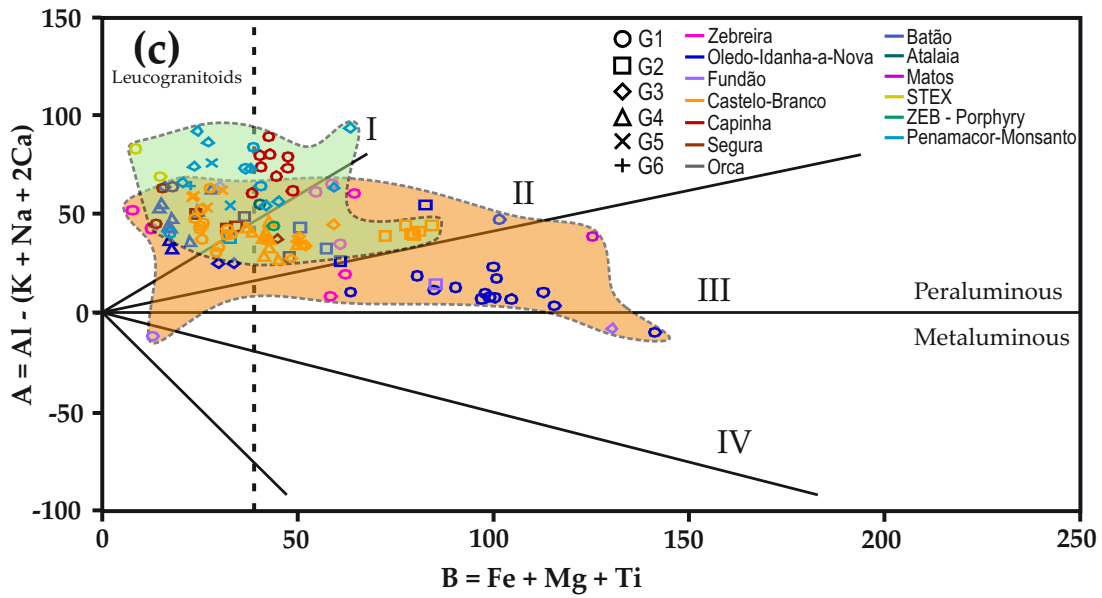
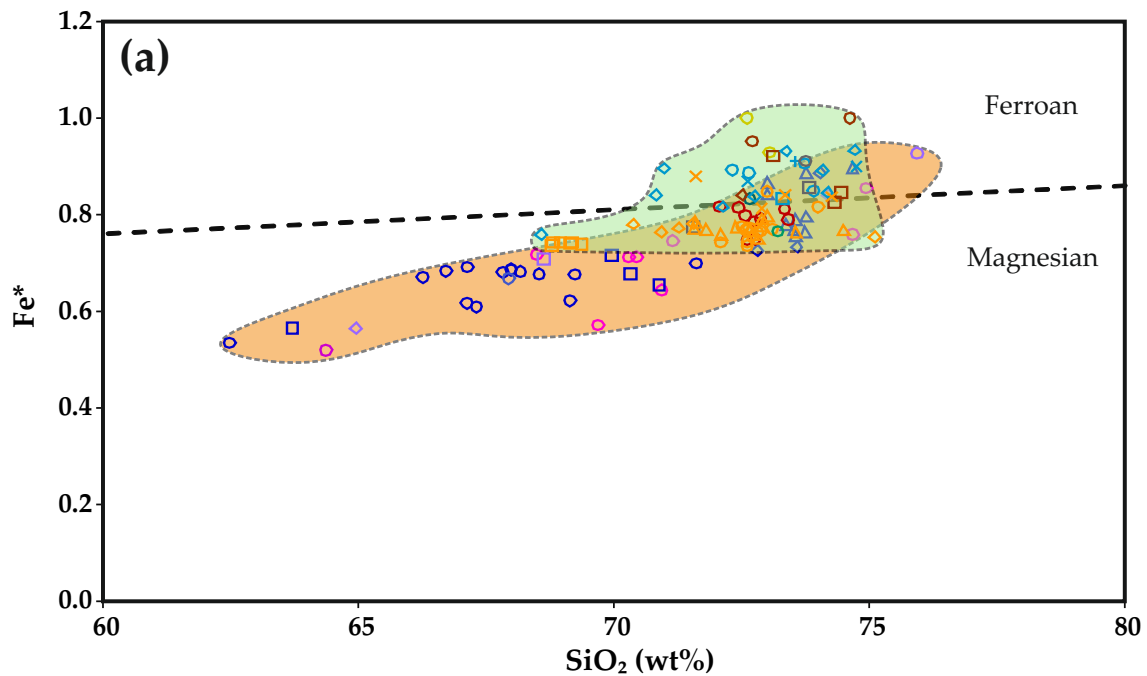


Figure 3. Cont.



**Figure 3.** Classification diagrams for the Cambrian–Ordovician (orange compositional field) and Variscan (green compositional field) granite suites. (a) Q-P diagram (adapted from [118]). ad—adamellite; dq—quartz diorite; gd—granodiorite; go—gabbro, diorite, anorthosite; gr—granite; mz—monzonite, mzdq—quartz monzodiorite, quartz monzogabbro; mzgo—monzogabbro, monzodiorite; mzq—quartz monzonite; s—syenite; sq—quartz syenite; to—tonalite, trondhjemite; (b) ASI vs. A/NK diagram (adapted from [119,120]); (c) A-B diagram (adapted from [118]). Sectors I, II, III—peraluminous rocks with muscovite > biotite, biotite > muscovite and biotite, respectively; Sector IV—metaluminous rocks with biotite + amphibole ± pyroxene. Symbols and colors in (c).



**Figure 4.** Cont.

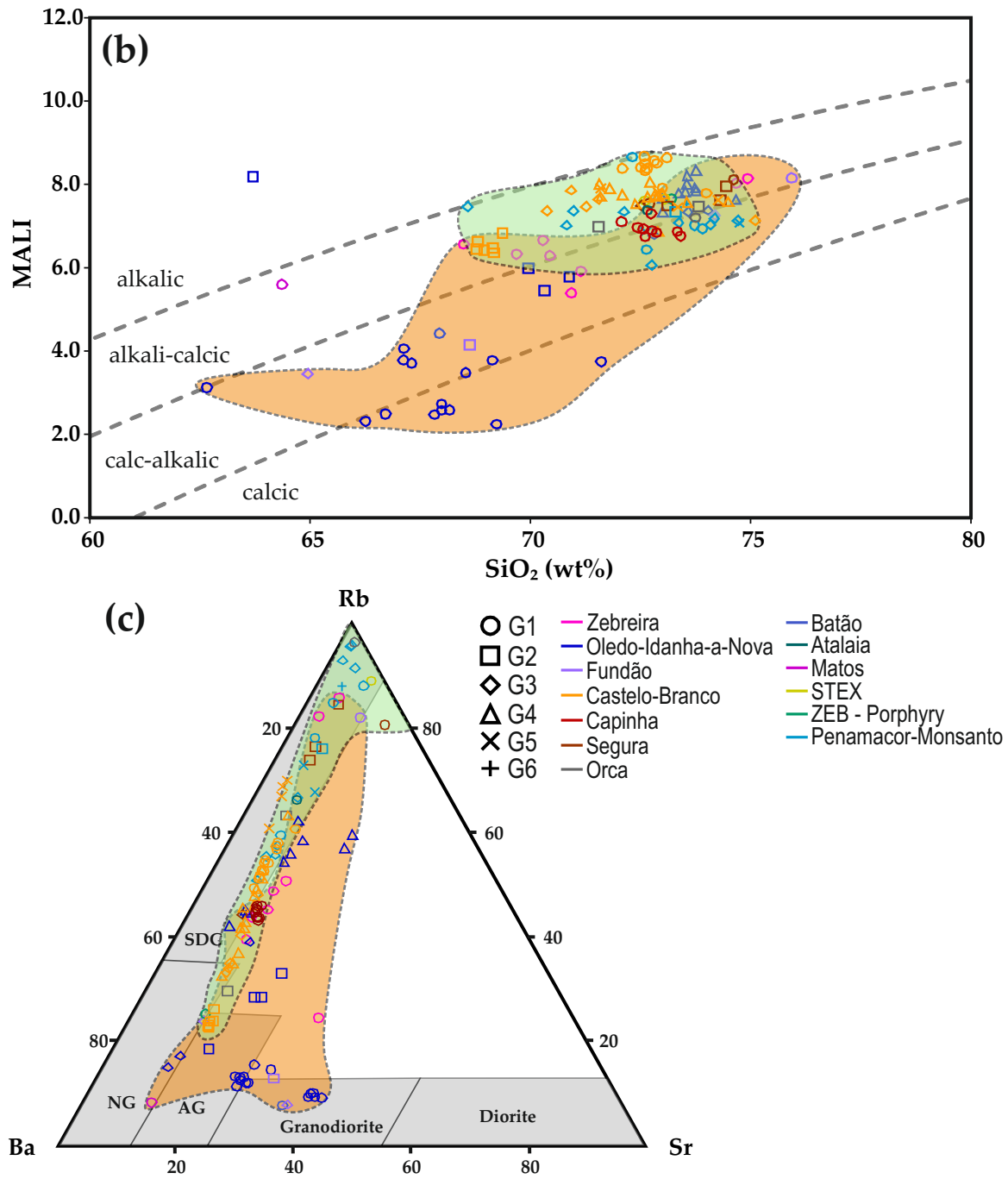


**Figure 4.** Classification diagrams for the Cambrian–Ordovician (orange compositional field) and Variscan (green compositional field) granite suites. (a) SiO<sub>2</sub> vs. Fe\* diagram (adapted from [121]); (b) SiO<sub>2</sub> (wt. %) vs. MALI diagram (adapted from [121]); (c) Ba-Rb-Sr ternary diagram (adapted from [122]). AG—Anomalous Granites; NG—Normal Granites; SDG—Strongly Differentiated Granites.

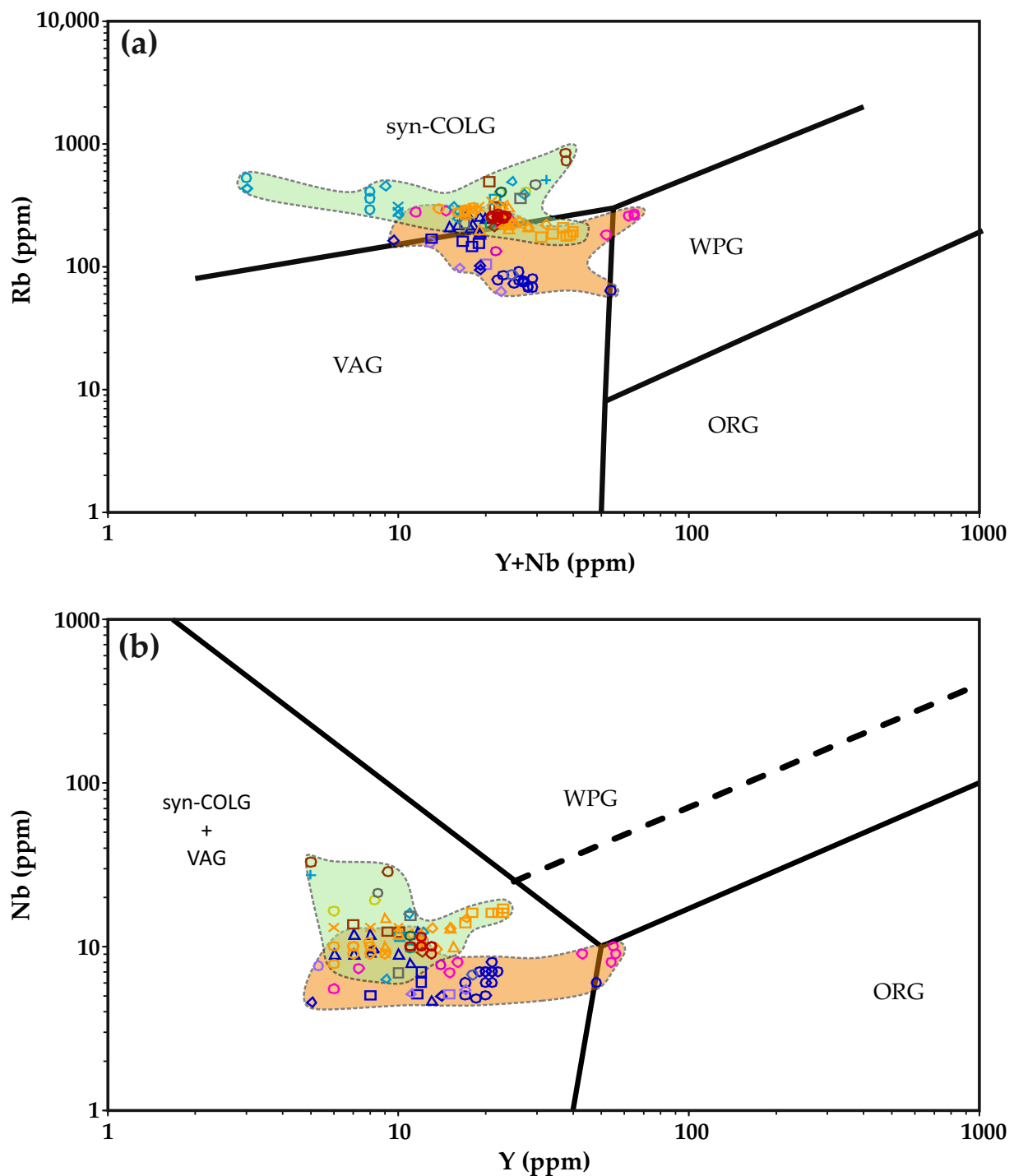


**Figure 5.** (a) Y+Nb vs. Rb; and (b) Y vs. Nb tectonic discrimination diagrams for the Cambrian–Ordovician (orange compositional field) and Variscan (green compositional field) granite suites (adapted from [123]). VAG—Volcanic Arc Granites; syn-COLG—syn-Collisional Granites; WPG—Within-Plate Granites; ORG—Ocean-Ridge Granites. Same symbols and colors as in Figure 4.

As previously mentioned, the deviations of the Cambrian–Ordovician granitoids towards Variscan magmatism compositions are exclusively registered in the late facies of the Zebreira, Oledo-Idanha-a-Nova, and Fundão plutons. These rocks are moderately peraluminous S-type (average ASI value of 1.23), monzogranite to granite rocks (Figure 3). They also present high SiO<sub>2</sub> (average content 73.9 wt. %), total alkalis (average content 8.34 wt. %), and Fe\* ratios (average value 0.82) values, thus corresponding to the calc-alkalic

to alkali-calcic granitic series and plotting in the fields of magnesian to ferroan granites (Figure 4a,b). As to their tectonic settings and magmatic differentiation degree, these facies display the compositional features of syn-collisional and strongly differentiated granites (Figures 4c and 5).

Considering the A-B classification diagram for felsic rocks of Debon and Lefort (1988) [118], modified by Cuney (2014) [124] and Romer and Pichavant (2020) [20], it is possible to classify the highly differentiated granitic rocks along the evolution path of the aluminum saturation index, during magmatic fractionation. This diagram considers Fe-Mg minerals and aluminosilicates (e.g., muscovite, topaz, cordierite, garnet, biotite, amphibole, pyroxene), and usually only the highly evolved rare-metal granites and aplite-pegmatite dykes deviate from the origin of the diagram (point of extreme fractional crystallization) to higher A values. The granite facies and aplite-pegmatite dykes of Argemela, Panasqueira, Segura, Oledo-Idanha-a-Nova, Orca, and Penamacor-Monsanto, follow the typical fractionation trend of S-type granites, falling mostly in the leucogranite field, near the RMG composition. The deviation from this general trend is essentially justified by the geochemical composition of the Panasqueira greisen, Argemela RMG and aplite-pegmatite dykes from Argemela and Segura that display variable A values, reflecting late magmatic-hydrothermal interaction and/or strongly peraluminous melt compositions capable of stabilizing muscovite, lepidolite, Li-Al-phosphates (montebrasite-amblygonite), and topaz (Figure 6).

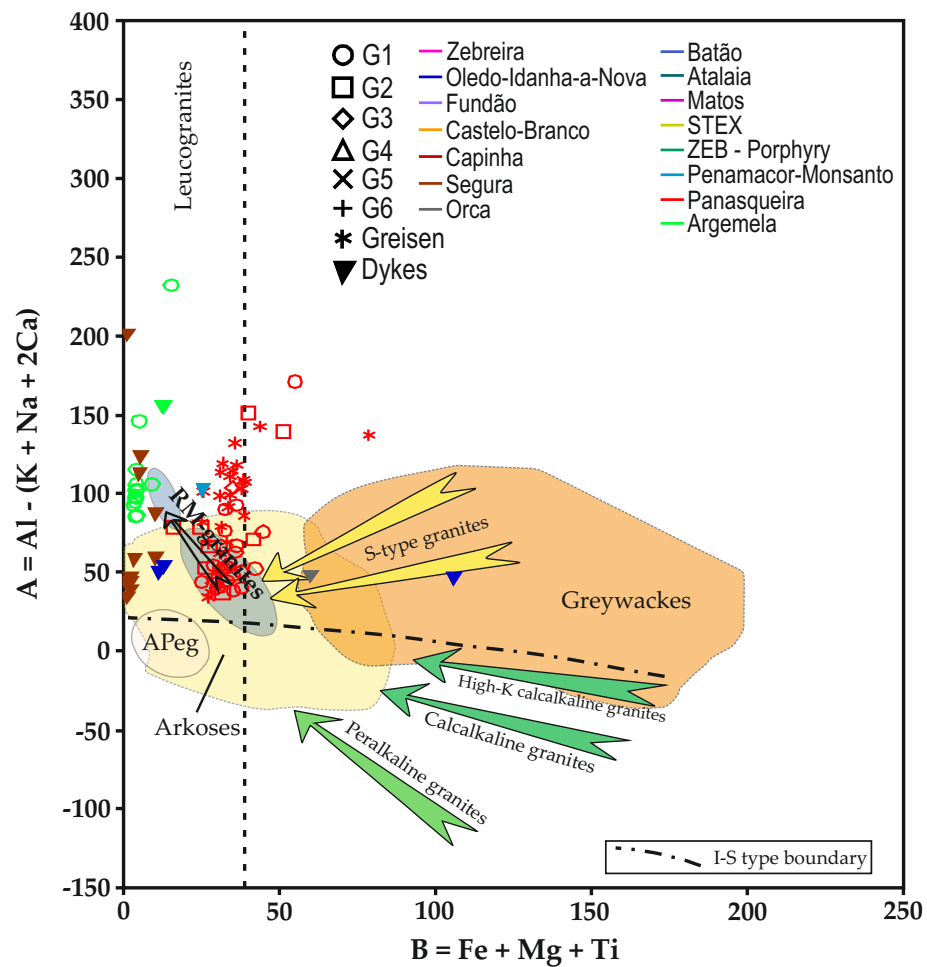


**Figure 6.** Modified A-B classification diagram for the highly differentiated granite facies and aplite-pegmatites dykes from Oledo-Idanha-a-Nova, Orca, Penamacor-Monsanto, Segura, Panasqueira and Argemela. APeg—aneatectic pegmatites; RM-granites—Rare Metal granites (adapted from [20,124]).

4.2. Trace Elements

The Upper Continental Crust-normalized (UCC) [125], multi-element patterns are drawn for the Cambrian–Ordovician and Variscan granitoids in Figure 7a,b. They are mostly characterized by positive anomalies in P, Li, B, Cs, Ta, and U, and negative anomalies in Ba, Zr, and Th, usually much more evident for the granitoids representing the Variscan magmatic event. In addition, the Variscan granitoid facies display positive anomalies in Be and Sn and negative anomalies in F, Rb, and Y. Regardless of the type of anomalies, these two magmatic sets show UCC-normalized patterns with substantial enrichment in P, F, Be, Li, B, Rb, Cs, Ta, Sn, W, and U, and depletion in Ba, Sr, Zr, Hf, Th, and Y, especially significant in the Variscan granite facies. The highly differentiated granite facies and aplite–pegmatite dykes are characterized by positive anomalies in P, Be, Li, Rb, Ta, Sn, Hf, and U, and negative anomalies in F, B, Ba, Zr, Th, and Y (Figure 7c). Besides similar relative enrichments and depletions to those observed in the granite facies from the Cambrian–Ordovician and Variscan magmatic events, the highly differentiated granite facies and aplite–pegmatite dykes also record very high enrichments in Nb. In general, all elemental anomalies are more pronounced in the differentiated granite facies and aplite–pegmatite dykes, especially those concerning P, F, Be, Li, Ta, and Sn enrichment.

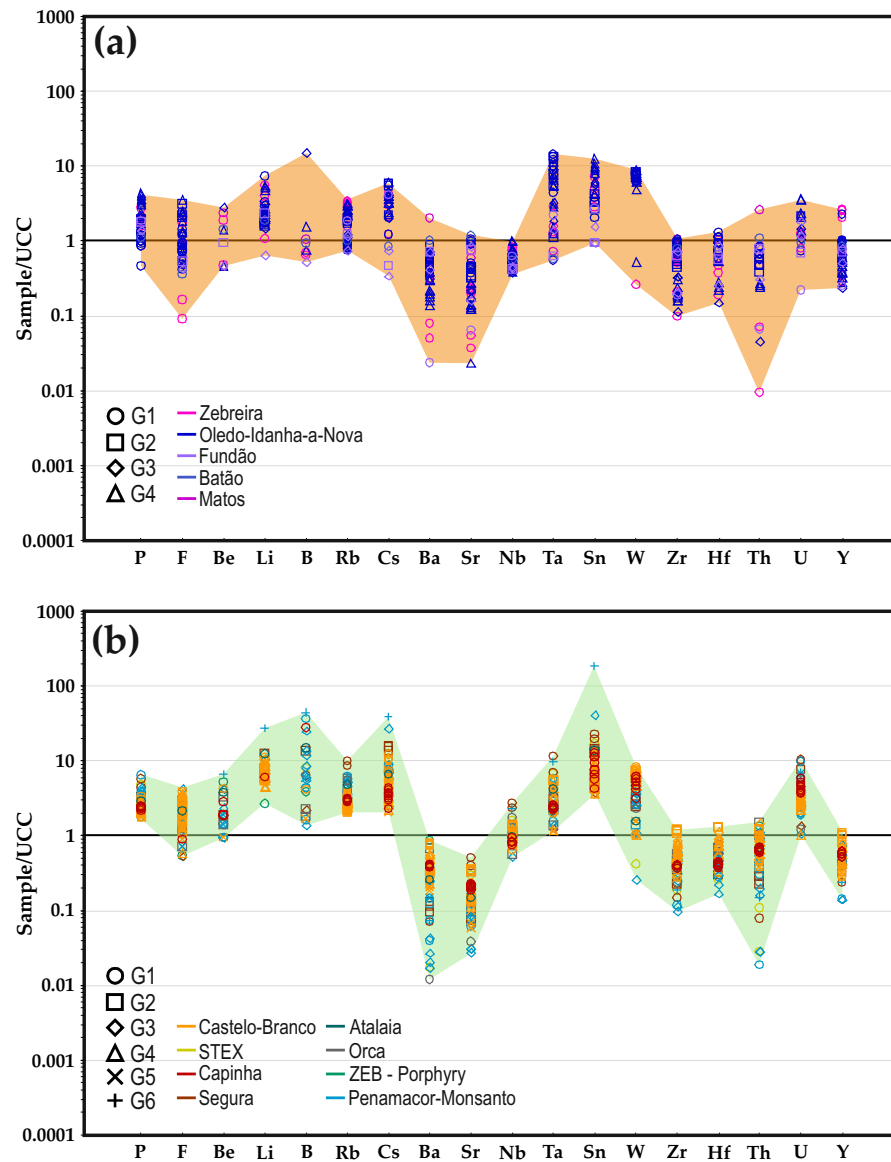
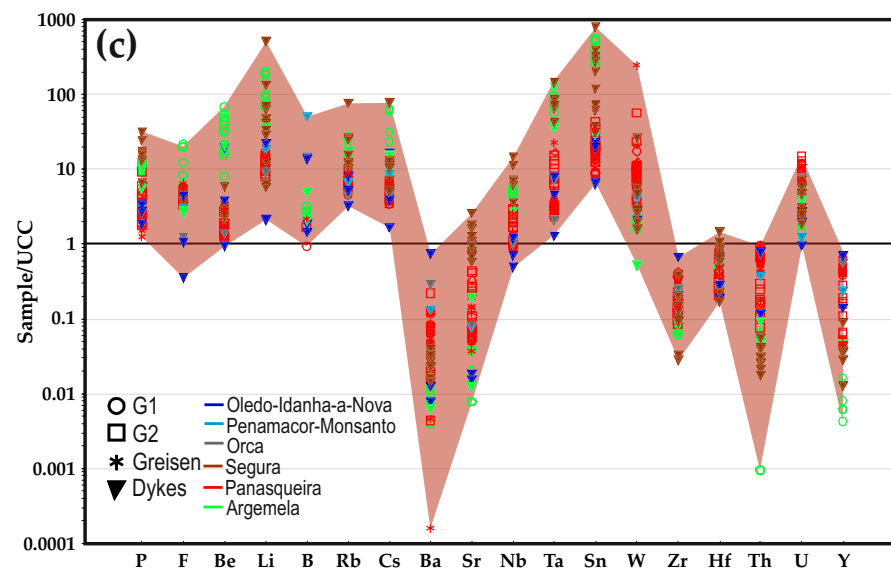


Figure 7. Cont.



**Figure 7.** Upper Continental Crust-normalized multi-element concentration patterns for the (a) Cambrian–Ordovician granitoids (orange compositional field); (b) Variscan granitoids (green compositional field); and (c) highly differentiated granite facies and aplite–pegmatite dykes (pink compositional field). Upper Continental Crust (UCC) normalization values after [125]. Symbols and colors in (c).

#### 4.3. Rare Earth Elements

Rare earth elements (REE) data are summarized in Table S2. The chondrite-normalized (CN) [126] patterns show that rocks representing the Cambrian–Ordovician and the Variscan magmatic events display wide REE concentration ranges ( $\Sigma\text{REE} = 10.4$  to  $172.0$  ppm and  $\Sigma\text{REE} = 8.9$  to  $194.6$  ppm, respectively), but present similar chondrite-normalized patterns (Figure 8a,b). Both patterns are negatively sloped, showing light rare earth elements (LREE) enrichments relative to heavy rare earth elements (HREE) ( $\text{La}/\text{Yb}_{\text{CN}} = 1.7$  to  $18.77$  and  $\text{La}/\text{Yb}_{\text{CN}} = 1.8$  to  $25.6$ , respectively), with different degrees of HREE fractionation ( $\text{Dy}/\text{Yb}_{\text{CN}} = 0.8$  to  $2.6$  and  $\text{Dy}/\text{Yb}_{\text{CN}} = 1.3$  to  $4.1$ , respectively) and negative Eu anomalies ( $\text{Eu}/\text{Eu}^* = 0.3$  to  $1.0$  and  $\text{Eu}/\text{Eu}^* = 0.1$  to  $0.6$ , respectively) that tend to be more pronounced in the samples from the Variscan granite suites. The similarities in REE fractionation observed in the samples from Cambrian–Ordovician and Variscan suites, with slight differences in the HREE, explain the comparable degrees of the tetrad effect, though Variscan granites record slightly higher values ( $\text{TE}_{1,3} = 0.95$  to  $1.20$  for the Cambrian–Ordovician suite;  $\text{TE}_{1,3} = 0.99$  to  $1.30$  for the Variscan suite). In this regard it should be noted that lowermost  $\Sigma\text{REE}$  whole-rock contents are typical of highly differentiated samples, conceivably representing extremely fractionated residual melts formed/extracted after the early crystallization of REE-incorporating minerals (such as monazite) in parental granitic magmas. Some of these samples were also lately subjected to significant compositional changes triggered by high-temperature hydrothermal processes, as discussed in Section 5.

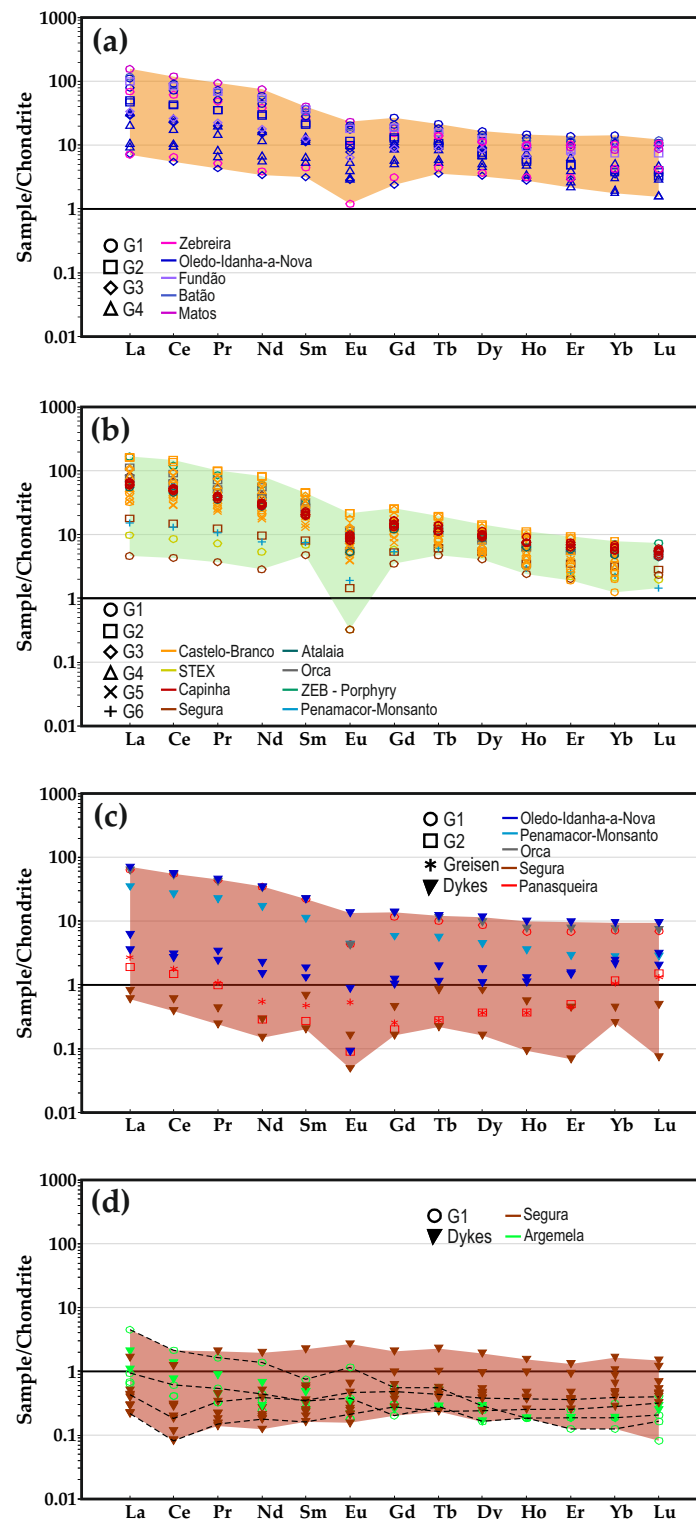


**Figure 8.** REE Chondrite-normalization diagram for the (a) Cambrian–Ordovician granitoids (orange compositional field); (b) Variscan granitoids (green compositional field); Highly differentiated granite facies and aplite–pegmatite dykes (red compositional field) with (c) M-type patterns; and (d) W-type patterns, highlighted by dashed lines. Chondrite normalization values after [126].

Considering the chondrite-normalized patterns of the highly differentiated granite facies and aplite–pegmatite dykes, it is possible to distinguish two main groups (Figure 8c). The first group includes the Panasqueira Greisen and Granite facies, the Segura Li-Sn lepidolite-bearing aplites, the Penamacor–Monsanto pegmatite, the Orca pegmatite, and the

Oledo-Idanha-a-Nova aplite–pegmatite dykes and is typified by M-type (convex) chondrite-normalized patterns. These felsic rocks have wide-ranging REE contents ( $\Sigma\text{REE} = 0.6$  to 83.8 ppm), negatively sloped chondrite-normalized patterns ( $\text{La}/\text{Yb}_{\text{CN}} = 1.5$  to 12.5), slightly flat HREE patterns ( $\text{Dy}/\text{Yb}_{\text{CN}} = 0.3$  to 1.9) and pronounced negative Eu anomalies ( $\text{Eu}/\text{Eu}^* = 0.1$  to 1.6, average value of 0.5), being characterized by significant degrees of tetrad effect ( $\text{TE}_{1,3} = 1.01$  to 1.38). The second group comprises the rare metal granite and aplite–pegmatite dykes from Argemela and the Li-phosphates-bearing pegmatite dykes from Segura, being mostly characterized by W-type (concave) chondrite-normalized patterns. These highly differentiated rocks have low REE contents ( $\Sigma\text{REE} = 0.5$  to 4.3 ppm), positively to negatively sloped chondrite-normalized patterns ( $\text{La}/\text{Yb}_{\text{CN}} = 0.4$  to 24.0), low HREE fractionation ( $\text{Dy}/\text{Yb}_{\text{CN}} = 0.5$  to 1.5), moderate negative to strongly positive Eu anomalies ( $\text{Eu}/\text{Eu}^* = 0.4$  to 1.8) and extremely low  $\text{TE}_{1,3}$  values (0.71 to 1.05), consistently documenting the absence of a tetrad effect [18]. The implication of considering two different geochemical groups and its relevance for the exploration of W-Sn-Li granite-related ore deposits will be discussed in the following section.

## 5. Discussion

### 5.1. Magmatic Differentiation and Metal Specialization: Correlation with $\text{TE}_{1,3}$

The degree of differentiation and metal specialization of the granitoid suites was necessary to evaluate before assessing the usefulness of the  $\text{TE}_{1,3}$  parameter as a marker of granitic magma differentiation and as an exploration tool for granite-related rare metal ore systems. For that purpose, (i) the Nb/Ta, K/Rb, Y/Ho, Sr/Eu, Eu/Eu\*, Zr/Hf, and Rb/Sr ratios were considered as geochemical magmatic differentiation markers; (ii) the values Nb/Ta < 5, K/Rb < 150, Y/Ho > 28, Sr/Eu > 200, and Eu/Eu\* < 0.1 were used as indicators of significant magmatic-hydrothermal processes [4,18,127]; and (iii) the representative compositions of granite suites with different degrees of differentiation and metal-enrichments from other sectors of the Variscan orogenic belt (Table S3) were plotted to ascertain the representative geochemical trends on the basis of a wide and robust dataset. The chosen reference granite suites include: the Cambrian–Ordovician Beira-Extremadura Batholith [128]; the Armorican Massif, the Erzgebirge–Fichtelgebirge, and Cornwall Variscan granites ([4] and references therein); the Variscan Penouta Sn-Ta-Nb RMG [129]; and several other Iberian Variscan granites ([4] and references therein, [130]).

Granite facies with low Nb/Ta ratios also tend to display low K/Rb, Eu/Eu\* and Zr/Hf ratios, and high Y/Ho, Sr/Eu, and Rb/Sr ratios (Figure 9), showing a clear correlation between the different element ratios. Moreover, a remarkable compositional similarity is observed between the studied samples and the published data for similar rocks from other Variscan crustal segments (Figure 9). Whereas most of the weakly peraluminous Cambrian–Ordovician rocks represent the less evolved facies, the highly peraluminous Variscan granite facies and late aplite–pegmatite dykes are strongly differentiated and significantly affected by magmatic-hydrothermal processes (Figure 9a–d,f). The most evolved rocks are the granite facies of Segura, Salvaterra do Extremo, Penamacor–Monsanto, Panasqueira, Argemela, and Penouta and the aplite–pegmatite dykes from Oledo-Idanha-a-Nova, Segura, Penamacor–Monsanto, and Argemela. Additionally, the Nb/Ta vs. Zr/Hf [19,127] and Rb/Sr vs. Sn [20,127] ratios can also be considered geochemical indicators of the fertility of granitic rocks, distinguishing barren granites from Sn-W(-U)-specialized granites and (Ta-Cs-Li-Nb-Be-Sn-W)-enriched/related granites. Cambrian–Ordovician magmatism is essentially characterized by barren granites, whereas Variscan magmatism tends to be more fertile, especially for Sn-W(-U) granite-related ore deposits. The more evolved rocks and those most affected by late magmatic-hydrothermal fluids display the specialized features of Ta-Cs-Li-Nb-Be-Sn-W granite-related ore systems. Among the samples of the latter suite, the granite facies of Argemela and Penouta, as well as the aplite–pegmatite dykes of Argemela and Segura, are the most specialized (Figure 9e,f). Granite differentiation, and subsequent compositional modifications ascribed to magmatic-hydrothermal processes,

have led to progressive enrichment in granitophile elements, such as Sn, Li, Nb, Ta, Be, and Cs (Figure 10a–f).

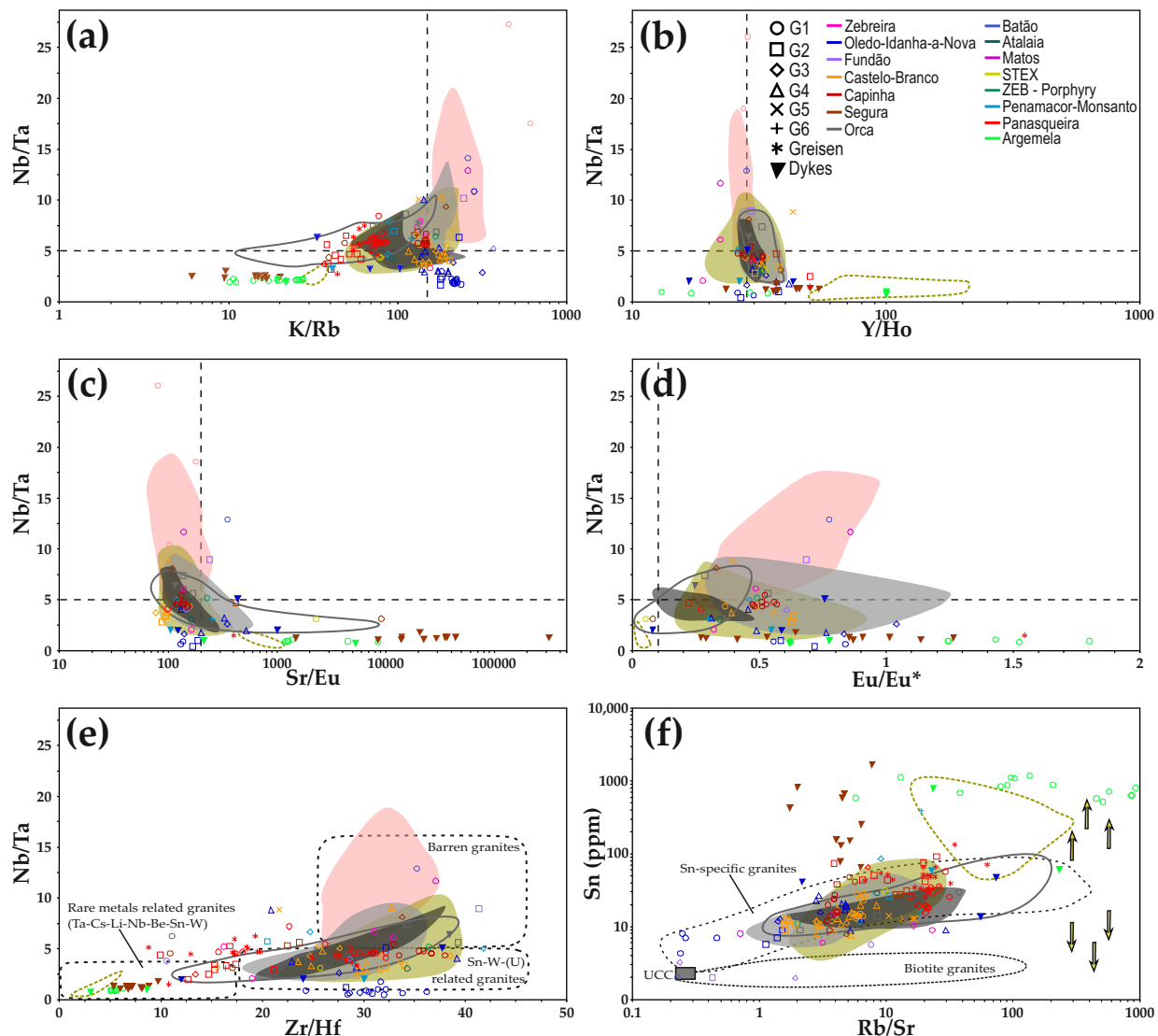


**Figure 9.** Diagrams showing the variation of key trace element ratios for granite facies exposed in the Segura–Panasqueira area, evidencing different degrees of differentiation, late-stage magmatic-hydrothermal interactions, and metal specialization. (a) K/Rb vs. Nb/Ta; (b) Y/Ho vs. Nb/Ta; (c) Sr/Eu vs. Nb/Ta; (d) Eu/Eu\* vs. Nb/Ta; (e) Zr/Hf vs. Nb/Ta diagram separating barren and ore-related peraluminous granites (adapted from [19]). (f) Rb/Sr vs. Sn diagram evidencing the enrichment in Sn with increasing degree of differentiation (adapted from [20]). This diagram discriminates biotite granites from Sn-specialized granites, and compositional deviations related to late-stage melt-hydrothermal transition (yellow arrows). These diagrams include the representative compositional fields of other granite suites, namely from: the Cambrian–Ordovician Beira-Extremadura batholith (pink compositional area, [128]); the Armorican Massif (grey compositional area, [4] and references therein); the Iberian Massif (greenish-yellow compositional area, [4] and references therein, [130] and references therein), the Erzgebirge–Fichtelgebirge (solid dark grey line, [4] and references therein); Cornwall (black compositional area, [4] and references therein) and the Penouta RMG (dashed greenish-yellow line, [4] and references therein). The black dashed lines represent reference values of Nb/Ta < 5, K/Rb < 150, Y/Ho > 28, Sr/Eu > 200 and Eu/Eu\* < 0.1, normally displayed by peraluminous granites that have experienced significant interaction with high-temperature hydrothermal fluids [4,18]. Symbols and colors in (b).

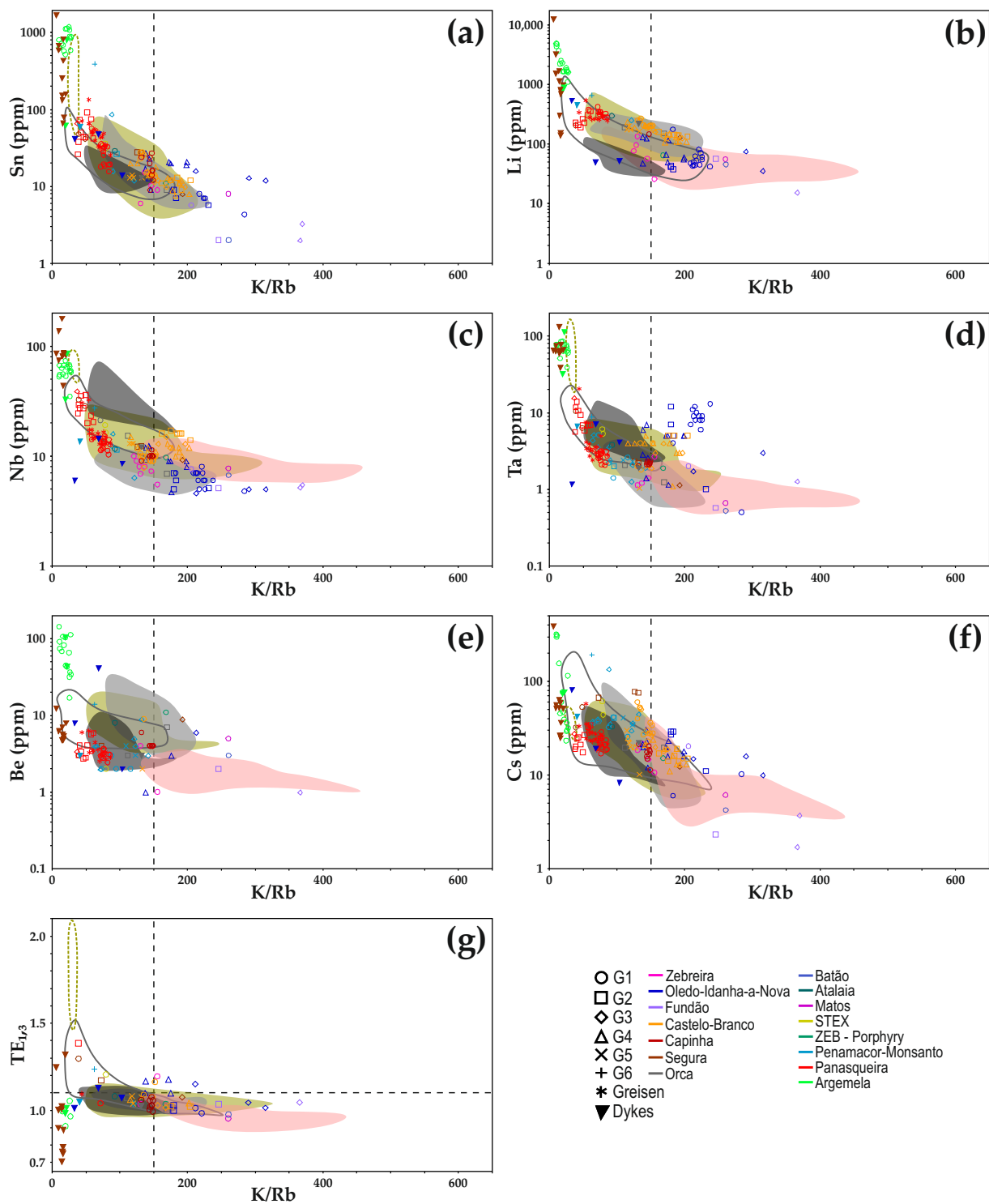


**Figure 10.** (a–f) Selected trace element contents vs. K/Rb ratios for the granite facies exposed across the Segura–Panasqueira area, evidencing different degrees of differentiation (K/Rb) and enrichment in common rare metals in granite-related ore systems (Sn, Li, Nb, Ta, Be, and Cs). It should be noted that the granite rocks in this study present low W contents ( $\leq 50.44$  ppm), often below the detection limits of the analytical methods used, and therefore W has not been considered. (g) K/Rb vs. TE<sub>1,3</sub>, showing the correlation between granite differentiation and the degree of the tetrad effect; Representative compositional fields for other granite suites are plotted as in Figure 9. Black dashed lines represent reference values of K/Rb < 150 and TE<sub>1,3</sub> > 1.1, usually displayed by peraluminous granites that have experienced significant interaction with high-temperature hydrothermal fluids [4,18].

The increase in  $TE_{1,3}$  values tends to correlate with magmatic differentiation and metal-enrichment, as documented by the contrast between the poorly differentiated Cambrian–Ordovician granite suites, with the lowest  $TE_{1,3}$  values ( $\leq 1.2$ ), and the Variscan granite facies, showing gradually higher  $TE_{1,3}$  (up to 2.1–Penouta RMG) (Figure 10g). Although the Li-phosphate-bearing Argemela RMG and the aplite–pegmatite dykes from Argemela and Segura present the highest differentiation degrees and metal enrichment, they deviate from this geochemical trend, showing no evidence of tetrad effect ( $TE_{1,3} < 1.1$ ). Moreover, it is worth highlighting that, based on the  $TE_{1,3}$  parameter there is a clear distinction between these Li-phosphate-bearing dykes and the lepidolite-bearing aplites from Segura, which follow the general trend. As suggested by Irber (1999) [18], the development of the lanthanide tetrad effect (M-type) with pronounced negative  $Eu^*$  in highly evolved granitic rocks implies the removal of a mirroring REE-pattern (W-type) with positive  $Eu^*$ , corresponding to a coexisting high-temperature aqueous fluid. Therefore, although most of the granite facies considered are characterized by the REE signatures of silicate melts with gradually higher degrees of differentiation, the Argemela RMG and the Li-phosphates-bearing aplite–pegmatite dykes from Argemela and Segura show compositional signatures comparable with those expected for high-temperature aqueous fluids, as indicated by the absence of the tetrad effect ( $TE_{1,3} < 1.1$ ) and by the tendency of  $Eu^*$  anomalies to be positive (Figure 9d).

### 5.2. The $TE_{1,3}$ as an Exploration Vector for Granite-Related Ore Systems

In many granite systems, differentiation leads to a gradual enrichment of fluxing components ( $H_2O$ , P, F, B) in the melt that, for extreme fractionation, might be completed by segregation of an  $H_2O$ -saturated melt and a high-temperature aqueous fluid [116,131–133]. Crystallization of highly evolved silicate melts coexisting with aqueous high-temperature fluids results in important changes in the geochemical behavior of many elements. During primary unmixing, rare metal concentrations are no longer exclusively controlled by ionic radius and charge but also by the partition between magma and the fluid phase [4,16,18,134]. Thus, to understand how the REE fractionation signatures in Li–Sn, W–Sn, and Sn–Ta–Nb granite-related ore systems are influenced by these magmatic-hydrothermal processes and relative predominance of P, F, and B, it is important to evaluate their correlation with  $TE_{1,3}$  (Figure 11). To this end, three main geochemical trends can be distinguished, as a function of the REE-bearing accessory minerals (e.g., apatite, monazite, zircon, xenotime, fluorite, and garnet). The  $TE_{1,3}$  value of the pristine melt may explain the features of the unmixed high-temperature aqueous fluid [18].

The first trend depicts magmatic-hydrothermal systems dominated by P and F ( $P + F \pm B$ ,  $P > F$ ) analogous to those typified by the Li–Sn Argemela RMG and the Li-phosphate-bearing aplite–pegmatites from Segura. In these peraluminous-high-phosphorus (PHP) systems, with high  $P_2O_5$  and Li contents (up to 4.76 wt. % and 1.27 wt. %, respectively) and low ranges of CaO ( $\leq 0.85$  wt. %), phosphate is firstly present as apatite, and the phosphorus excess at a given CaO content formed a phosphate from the amblygonite-montebbrasite series. The strong negative correlation between  $P_2O_5$  and  $TE_{1,3}$  suggest that Na–Li phosphates incorporate REE from the fluid.

The second geochemical trend describes peraluminous-high-phosphorus magmatic-hydrothermal systems dominated by F and P ( $F + P \pm B$ ,  $F > P$ ), comparable to those represented by the W–Sn Panasqueira Granite facies and the Li–Sn, lepidolite-bearing aplites from Segura. These highly evolved rocks have slightly higher contents of F (up to 2300 ppm) and CaO (up to 1.7 wt. %) and lower  $P_2O_5$  contents ( $\leq 1.94$  wt. %), ordinarily expressed by the presence of fluor-apatite. In such cases, Li is usually incorporated in micas and not in phosphate. For these magmatic-hydrothermal systems, the typically high  $TE_{1,3}$  values match those of highly evolved silicate melts interacting with aqueous fluids (up to 1.4), and fluor-apatite acts as the primary REE-bearing mineral, as suggested by the positive correlation of  $P_2O_5$  and F with  $TE_{1,3}$ .

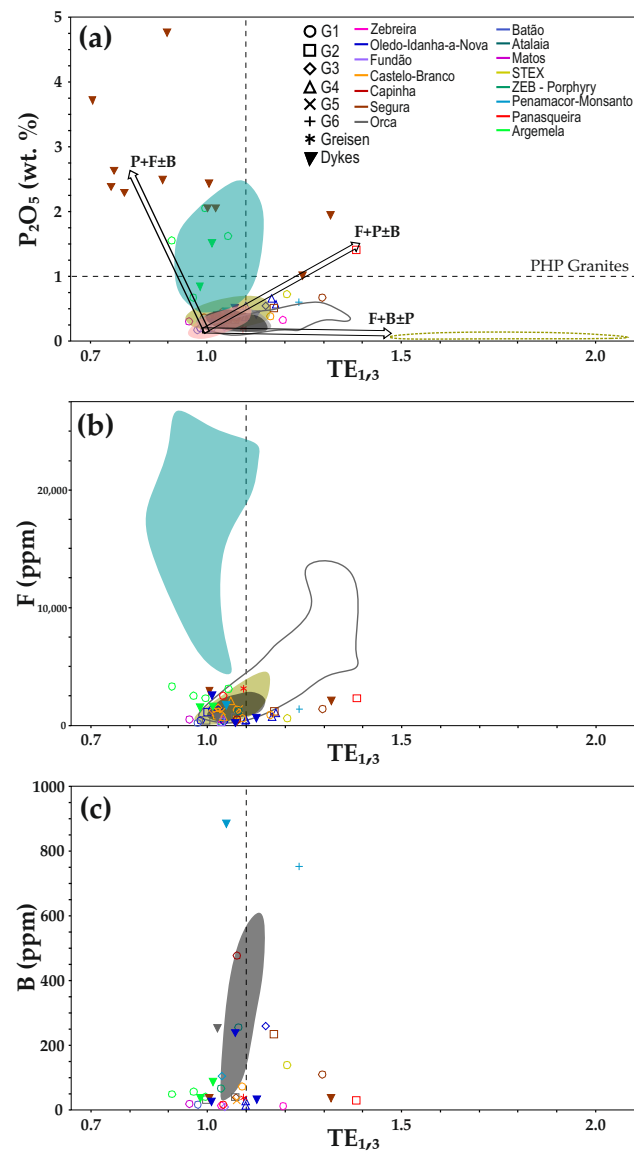


**Figure 11.** Variation of the tetrad effect ( $TE_{1,3}$ ) vs. (a)  $P_2O_5$  (wt. %), (b) F (ppm), and (c) B (ppm), showing the influence of the increasing concentration in fluxing elements on REE fractionation. Three main compositional trends are distinguished, representing magmatic-hydrothermal systems related to different types of mineralization: (i) Peraluminous High-Phosphorus Li-Sn magmatic-hydrothermal systems dominated by  $P + F \pm B$  ( $P > F$ ), in which Li is primarily incorporated in phosphate mineral phases; (ii) Peraluminous High-Phosphorus W-Sn-Li magmatic-hydrothermal systems dominated by  $F + P \pm B$  ( $F > P$ ) and variably enriched in Li-bearing micas; and (iii) Peraluminous Low-Phosphorus Sn-Nb-Ta magmatic-hydrothermal systems dominated by  $F + B \pm P$  ( $F > B$ ). Representative compositional fields of granitoid suites are plotted: the Cambrian–Ordovician Beira-Extremadura batholith (pink compositional area [128]); the Armorican Massif (grey compositional area [4], and references therein); the Iberian Massif (greenish-yellow compositional area [4], and references therein [130], and references therein); Erzgebirge–Fichtelgebirge (solid dark grey line [4], and references therein); Cornwall (black compositional area, [4] and references therein), the Penouta RMG (dashed greenish-yellow line [4], and references therein) and Beauvoir (blue compositional area). Black dashed lines represent reference values of  $TE_{1,3} > 1.1$  normally displayed by peraluminous granites that show effects of significant interaction with high-temperature aqueous fluids [4,18]. Due to incomplete analytical data, samples from the Beira-Extremadura batholith, the Iberian Massif, Erzgebirge–Fichtelgebirge, Cornwall and the Penouta RMG are not plotted on all diagrams. For the same reason, the Beauvoir data are only plotted in the diagrams (a,b) of this figure. Symbols and colors in (a).

The third compositional trend describes peraluminous-low-phosphorus (PLP) magmatic-hydrothermal systems, dominated by F and B ( $F + B \pm P$ ,  $F > B$ ), as those illustrated by the topaz-, tourmaline-, and garnet-bearing granites related to Sn-Ta-Nb ore systems such as the cases of the Penouta RMG and the granite facies of Erzgebirge–Fichtelgebirge and of Penamacor–Monsanto. These highly differentiated rocks are characterized by the highest  $TE_{1,3}$  values (up to 2.1), probably inherited from the highly evolved silicate melt coexisting with a late magmatic-hydrothermal fluid; topaz and other F-rich phases are the prevalent mineral proxy, as shown by the co-variation between F contents and  $TE_{1,3}$  values.

In summary, the degree of the lanthanide tetrad effect is a useful whole-rock geochemical fingerprint of granite differentiation for silicate magmatic-hydrothermal systems dominated by F and B and with strong granitic magma REE signatures. In such cases the  $TE_{1,3}$  correlates positively to increasing granite differentiation. For late magmatic-hydrothermal systems dominated by P and F, represented by the Li-phosphate-bearing rare-metal granites and the aplite–pegmatites dykes, the negative correlation between high degree of differentiation and low values of the degree of the tetrad effect ( $TE_{1,3} < 1.1$ ) suggest that these rocks have strong REE signatures of high-temperature aqueous fluids. It is also recommended that the  $TE_{1,3}$  values may be considered an exploration vector for different types of granite-related ore systems when plotted against  $P_2O_5$  (wt. %). Magmatic-hydrothermal systems may be therefore divided into three distinct trends: (i) Li-Sn, Li-phosphate-bearing granite-related ore systems; (ii) W-Sn-Li, fluorapatite- and lepidolite-bearing granite-related ore systems; and (iii) Sn-Nb-Ta topaz-, tourmaline- and garnet-bearing granite-related ore systems.

## 6. Conclusions

The comprehensive geochemical characterization of the main plutons and late aplite–pegmatite dykes exposed across the Segura–Panasqueira Sn-W-Li belt (Central-Iberian Zone) show that the Cambrian–Ordovician and Carboniferous–Permian granite suites: (i) display different degrees of differentiation and metal-enrichment, and (ii) their compositional features compare well with data published for similar rocks from other Variscan segments. Increasing  $TE_{1,3}$  values (up to 1.4) correlate with magmatic differentiation and metal-enrichment, and the Carboniferous–Permian granites are more differentiated, and metal specialized. The Li-Sn ore systems, Li-phosphate-bearing, Argemela RMG and aplite–pegmatite dykes from Segura deviate from this geochemical trend, displaying  $TE_{1,3}$  values  $< 1.1$ , but also high  $P_2O_5$  contents. It is then suggested that  $TE_{1,3}$  values and  $P_2O_5$  (wt. %) contents can be used together to distinguish three different magmatic-hydrothermal systems: (i) dominated by  $P + F \pm B$  ( $P > B$ ), with strong aqueous high-temperature REE signatures, and related to peraluminous-high-phosphorus Li-Sn granites and Li-phosphates-bearing aplite–pegmatite dykes ( $TE_{1,3} < 1.1$ ); (ii) dominated by  $F + P \pm B$  ( $F > P$ ) and related to W-Sn-Li peraluminous-high-phosphorus granites and lepidolite-bearing aplite–pegmatite dykes ( $TE_{1,3}$  up to 1.4); and (iii) dominated by  $F + B \pm P$  ( $F > B$ ) and related to peraluminous-low-phosphorus Sn-Ta-Nb granites ( $TE_{1,3}$  up to 2.1). Such data also suggest that the degree of the lanthanide tetrad effect can be a useful geochemical fingerprint of granite differentiation and an exploration vector for different granite-related ore systems.

**Supplementary Materials:** The following supporting information can be downloaded at: <https://www.mdpi.com/article/10.3390/min12091067/s1>, Table S1: Whole-rock geochemical data; Table S2: Rare earth elements data; Table S3: Variscan granites whole-rock geochemical data.

**Author Contributions:** I.M., fieldwork, geological mapping, sampling and sample preparation, conceptualization, numerical handling of analytical data, data interpretation and writing (original draft preparation, review, and editing); A.M., fieldwork, geological mapping, sampling, conceptualization, numerical handling of analytical data, data interpretation, writing (review and editing), and funding acquisition; M.C., sampling, data interpretation, writing (review and editing) and funding acquisition; M.C.B., sampling, data interpretation, writing (review and editing) and funding acquisition;

I.R.d.C., data interpretation, writing (review and editing) and funding acquisition; Í.D.d.S., fieldwork, geological mapping, sampling, writing (review and editing), and funding acquisition; M.G., writing (review and editing) and funding acquisition. All authors have read and agreed to the published version of the manuscript.

**Funding:** This work was supported by Fundação para a Ciência e Tecnologia, I.P./MCTES through national funds (PID-DAC)—UIDB/50019/2020 and PD/BD/142783/2018, being also a contribution of MOSTMEG project (ERA-MIN/0002/2019), <http://mostmeg.rd.ciencias.ulisboa.pt/> (accessed on 21 August 2022). French authors benefited from Agence Nationale de la Recherche funding through MOSTMEG and also from the programmes of the Labex RESSOURCES21 under the reference ANR-10-LABX-21-RESSOURCES21 supported by the Agence Nationale de la Recherche through the national programme “Investissements d’avenir”.

**Acknowledgments:** The authors are thankful to Beralt Tin and Wolfram S.A. for permitting the access to SCB2 drill core from the Panasqueira Mine area. The administrative support of Célia Lee is also warmly acknowledged. This work is a contribution to IDL Research Group 3 (Solid Earth Dynamics, Hazards and Resources). The constructive comments and suggestions of three anonymous Reviewers were much appreciated.

**Conflicts of Interest:** The authors declare no conflict of competing financial interests or personal relationships that could have influenced the work reported in this paper.

## References

1. Linnen, R.L.; Van Lichtervelde, M.; Černý, P. Granitic pegmatites as sources of strategic metals. *Elements* **2012**, *8*, 275–280. [[CrossRef](#)]
2. Gunn, G. *Critical Metals Handbook*; John Wiley & Sons, Ltd.: Hoboken, NJ, USA, 2013.
3. Dehainea, Q.; Filippova, L.O.; Glass, H.J.; Rollinson, G. Rare-metal granites as a potential source of critical metals: A geometallurgical case study. *Ore Geol. Rev.* **2019**, *104*, 384–402. [[CrossRef](#)]
4. Ballouard, C.; Massuyeau, M.; Elburg, M.A.; Tappe, S.; Viljoen, F.; Brandenburg, J. The magmatic and magmatic-hydrothermal evolution of felsic igneous rocks as seen through Nb-Ta geochemical fractionation, with implications for the origins of rare-metal mineralizations. *Earth Sci. Rev.* **2020**, *203*, 103115. [[CrossRef](#)]
5. Cerný, P.; Blevin, P.L.; Cuney, M.; London, D. Granite-related ore deposits. In *Economic Geology*; Hedenquist, J.W., Thompson, J.F.H., Goldfarb, R.J., Richards, J.R., Eds.; Society of Economic Geologists, Inc.: Littleton, CO, USA, 2005; Volume 100th Anniversary, pp. 337–370.
6. Sami, M.; Ntaflos, T.; Farahat, E.S.; Mohamed, H.A.; Ahmed, A.F.; Hauzenberger, C. Mineralogical, geochemical and Sr-Nd isotopes characteristics of fluorite-bearing granites in the Northern Arabian-Nubian Shield, Egypt: Constraints on petrogenesis and evolution of their associated rare metal mineralization. *Ore Geol. Rev.* **2017**, *88*, 1–22. [[CrossRef](#)]
7. Schuilig, R.D. Tin belts on the continents around the Atlantic Ocean. *Econ. Geol.* **1967**, *62*, 540–550. [[CrossRef](#)]
8. Derré, C. Caractéristiques de la distribution des gisements à étain et tungstène dans l’ouest de l’Europe. *Miner. Depos.* **1982**, *17*, 55–77. [[CrossRef](#)]
9. Marignac, C.; Cuney, M. Ore deposits of the French Massif Central: Insight into the metallogeny of the Variscan collision belt. *Miner. Depos.* **1999**, *34*, 472–504. [[CrossRef](#)]
10. Blundell, D.; Arndt, N.; Cobbold, P.R.; Heinrich, C. Geodynamics and ore deposit evolution in Europe. *Ore Geol. Rev.* **2005**, *27*, 345. [[CrossRef](#)]
11. De Vos, W.; Batista, M.J.; Demetriades, A.; Duris, M.; Lexa, J.; Lis, J.; Marsina, K.; O’Connor, P.J. Metallogenic mineral provinces and world class ore deposits in Europe. In *IUSGS/IAGC Global Geochemical Baselines*; EuroGeoSurveys: Brussels, Belgium, 2005.
12. Kerrich, R.; Goldfarb, R.J.; Richards, J.P. Metallogenic provinces in an evolving geodynamic framework. In *Economic Geology*; Hedenquist, J.W., Thompson, J.F.H., Goldfarb, R.J., Richards, J.R., Eds.; Society of Economic Geologists, Inc.: Littleton, CO, USA, 2005; Volume 100th Anniversary, pp. 1097–1136.
13. Romer, R.L.; Thomas, R.; Stein, H.J.; Rhede, D. Dating multiply overprinted Sn-mineralized granites—examples from the Erzgebirge, Germany. *Miner. Depos.* **2007**, *42*, 337–359. [[CrossRef](#)]
14. Harlaux, M.; Romer, R.L.; Mercadier, J.; Morloti, C.; Marignac, C.; Cuney, M. 40 Ma of hydrothermal W mineralization during the Variscan orogenic evolution of the French Massif Central revealed by U-Pb dating of wolframite. *Miner. Depos.* **2018**, *53*, 21–51. [[CrossRef](#)]
15. Gourcerol, B.; Gloaguen, E.; Melleton, J.; Tudur, J.; Galiegue, X. Re-assessing the European lithium resource potential—A review of hard-rock resources and metallogeny. *Ore Geol. Rev.* **2019**, *109*, 494–519. [[CrossRef](#)]
16. Bau, M. Controls on the fractionation of isovalent trace elements in magmatic and aqueous systems: Evidence from Y/Ho, Zr/Hf, and lanthanide tetrad effect. *Contrib. Mineral. Petrol.* **1996**, *123*, 323–333. [[CrossRef](#)]
17. Bau, M. The lanthanide tetrad effect in highly evolved felsic igneous rocks—A reply to the comment by Y. Pan. *Contrib. Mineral. Petrol.* **1997**, *128*, 409–412. [[CrossRef](#)]

18. Irber, W. The lanthanide tetrad effect and its correlation with K/Rb, Eu/Eu\*, Sr/Eu, Y/Ho, and Zr/Hf of evolving peraluminous granite suites. *Geochim. Cosmochim. Acta* **1999**, *63*, 489–508. [[CrossRef](#)]
19. Ballouard, C.; Poujol, M.; Boulvais, P.; Branquet, Y.; Tartèse, R.; Vignerresse, J.L. Nb-Ta fractionation in peraluminous granites: A marker of the magmatic-hydrothermal transition. *Geology* **2016**, *44*, 231–234. [[CrossRef](#)]
20. Romer, R.L.; Pichavant, M. Rare metal (Sn, W, Ta-Nb, Li) granites and pegmatites. In *Encyclopedia of Geology*, 2nd ed.; Alderton, D., Elias, S.A., Eds.; Academic Press: Cambridge, MA, USA, 2020; pp. 840–846.
21. Masuda, A.; Kawakami, O.; Dohmoto, Y.; Takenaka, T. Lanthanide tetrad effects in nature: Two mutually opposite types W and M. *Geochem. J.* **1987**, *21*, 119–124. [[CrossRef](#)]
22. Masuda, A.; Ikeuchi, Y. Lanthanide tetrad effect observed in marine environments. *Geochem. J.* **1978**, *13*, 19–22. [[CrossRef](#)]
23. Masuda, A.; Akagi, T. Lanthanide tetrad effect observed in leucogranites from China. *Geochem. J.* **1990**, *23*, 245–253. [[CrossRef](#)]
24. Akagi, T.; Nakai, S.; Shimizu, H.; Masuda, A. Constraints on the geochemical stage causing tetrad effect in kimuraite: Comparative studies on kimuraite and its related rocks, from REE pattern and Nd isotope ratio. *Geochem. J.* **1996**, *30*, 139–144. [[CrossRef](#)]
25. Yang, W.; Niu, H.; Shan, Q.; Sun, W. Geochemistry of magmatic and hydrothermal zircon from the highly evolved Baerzhe alkaline granite: Implications for Zr–REE–Nb mineralization. *Miner. Depos.* **2014**, *49*, 451–470. [[CrossRef](#)]
26. Badanina, E.V.; Sitnikova, M.A.; Gordienko, V.V.; Melcher, F.; Gäbler, H.E.; Lodziak, J.; Syritso, L.F. Mineral chemistry of columbite-tantalite from spodumene pegmatites of Kolmozero, Kola Peninsula (Russia). *Ore Geol. Rev.* **2015**, *64*, 720–735. [[CrossRef](#)]
27. Peretyazhako, I.S.; Savina, E.A. Tetrad effects in the rare earth element patterns of granitoid rocks as an indicator of fluoride-silicate liquid immiscibility in magmatic systems. *Petrology* **2010**, *18*, 514–543. [[CrossRef](#)]
28. Monecke, T.; Kempe, U.; Monecke, J.; Sala, M.; Wolf, D. Tetrad effect in rare earth element distribution patterns: A method of quantification with application to rock and mineral samples from granite-related rare metal deposits. *Geochim. Cosmochim. Acta* **2002**, *66*, 1185–1196. [[CrossRef](#)]
29. Monecke, T.; Dulski, P.; Kempe, U. Origin of convex tetrads in rare earth element patterns of hydrothermally altered siliceous igneous rocks from the Zinnwald Sn–W deposit, Germany. *Geochim. Cosmochim. Acta* **2007**, *71*, 335–353. [[CrossRef](#)]
30. Pan, Y.M. Controls on the fractionation of isovalent trace elements in magmatic and aqueous systems: Evidence from Y/Ho, Zr/Hf, and lanthanide tetrad effect—A discussion of the article by M. Bau (1996). *Contrib. Mineral. Petrol.* **1997**, *128*, 405–408. [[CrossRef](#)]
31. Pan, Y.M.; Breaks, F.W. Rare-earth elements in fluorapatite, Separation Lake area, Ontario; evidence for S-type granite-rare-element pegmatite linkage. *Can. Mineral.* **1997**, *35*, 659–671.
32. Ribeiro, A.; Iglesias, M.; Ribeiro, M.; Pereira, E. Modèle géodynamique des Hercynides Ibériques. *Comun. Serv. Geol. Port.* **1983**, *64*, 191–214.
33. Ribeiro, A.; Quesada, C.; Dallmeyer, R. Geodynamic evolution of the Iberian Massif. In *Pre-Mesozoic Geology of Iberia*; Springer: Berlin, Germany, 1990; pp. 399–409.
34. Ribeiro, A.; Munhá, J.; Dias, R.; Mateus, A.; Pereira, E.; Ribeiro, M.L.; Fonseca, P.; Araújo, A.; Oliveira, J.T.; Romão, J.; et al. Geodynamic evolution of the SW Europe Variscides. *Tectonics* **2007**, *26*. [[CrossRef](#)]
35. Martínez Catalán, J.R.; Rubio Pascual, F.J.; Díez Montes, A.; Díez Fernández, R.; Gómez Barreiro, J.; Dias da Silva, Í.; González Clavijo, E.; Ayarza, P.; Alcock, J.E. The late Variscan HT/LP metamorphic event in NW and Central Iberia: Relationships to crustal thickening, extension, orocline development and crustal evolution. *Lond. Geol. Soc.* **2014**, *405*, 225–247. [[CrossRef](#)]
36. Dias, R.; Ribeiro, A.; Romão, J.; Coke, C.; Moreira, N. A review of the arcuate structures in the Iberian Variscides; constraints and genetic models. *Tectonophysics* **2016**, *681*, 170–194. [[CrossRef](#)]
37. Ribeiro, A. Contribution à l'étude tectonique de Trás-os-Montes Oriental. *Comun. Serv. Geol. Port.* **1974**, *24*, 1–168.
38. Noronha, F.; Ramos, J.; Rebelo, J.; Ribeiro, A.; Ribeiro, M. Essai de corrélation des phases de déformation hercynienne dans le Nord-Ouest Péninsulaire. *Bol. Soc. Geol. Port.* **1979**, *21*, 227–237.
39. Dias, R.; Ribeiro, A. The Ibero-Armorican Arc: A collision effect against an irregular continent? *Tectonophysics* **1995**, *246*, 113–128. [[CrossRef](#)]
40. Azevedo, M.; Aguado, B. Origem e instalação de granitóides variscos na Zona Centro-Ibérica. In *Geologia de Portugal. Geologia Pré-Mesozoica de Portugal*; Escolar Editora: Lisbon, Portugal, 2013; Volume 1, pp. 377–401.
41. Azor, A.; Dias da Silva, Í.; Gómez Barreiro, J.; González-Clavijo, E.; Martínez Catalán, J.R.; Simancas, J.F.; Martínez Poyatos, D.; Pérez-Cáceres, I.; González Lodeiro, F.; Expósito, I.; et al. Deformation and Structure. In *The Geology of Iberia: A Geodynamic Approach, Volume 2, The Variscan Cycle*; Regional Geology Reviews; Springer: Gewerbestrasse, Switzerland, 2019; Volume 1, pp. 307–348.
42. Dallmeyer, R.D.; Martínez-Catalán, J.R.; Arenas, R.; Gil-Ibarguchi, J.I.; Gutiérrez-Alonso, G.; Farias, P.; Bastida, F. Diachronous Variscan tectonothermal activity in the NW Iberian Massif; evidence from <sup>40</sup>Ar/<sup>39</sup>Ar dating of regional fabrics. *Tectonophysics* **1997**, *277*, 307–337. [[CrossRef](#)]
43. Díez Fernández, R.; Pereira, M.F. Extensional orogenic collapse captured by strike-slip tectonics: Constraints from structural geology and U-Pb geochronology of the Pinhel shear zone (Variscan orogen, Iberian Massif). *Tectonophysics* **2016**, *691*, 290–310. [[CrossRef](#)]

44. Pereira, M.F.; Díez Fernández, R.; Gama, C.; Hofmann, M.; Gärtner, A.; Linnemann, U. S-type granite generation and emplacement during a regional switch from extensional to contractional deformation (Central Iberian Zone, Iberian autochthonous domain, Variscan Orogeny). *Int. J. Earth Sci.* **2018**, *107*, 251–267. [[CrossRef](#)]
45. Noronha, F.; Ribeiro, M.; Almeida, A.; Dória, A.; Guedes, A.; Lima, A.; Martins, H.; Sant’Ovaia, H.; Nogueira, P.; Martins, T.; et al. Jazigos filonianos hidrotermais e aplitopegmatíticos espacialmente associados a granitos (Norte de Portugal). In *Geologia de Portugal: Geologia Pré-Mesozoica de Portugal*; Escolar Editora: Lisbon, Portugal, 2013; Volume 1, pp. 403–438.
46. Ribeiro, A.; Antunes, M.T.; Ferreira, M.P.; Rocha, R.B.; Soares, A.F.; Zbyszewski, G.; Almeida, F.M.; Carvalho, D.; Monteiro, J.H. Introduction à la Géologie Générale du Portugal. *Serv. Geol. Port.* **1979**, 1–114.
47. Dias da Silva, Í.; González Clavijo, E.; Díez-Montes, A. The collapse of the Variscan belt: A Variscan lateral extrusion thin-skinned structure in NW Iberia. *Int. Geol. Rev.* **2021**, *63*, 659–695. [[CrossRef](#)]
48. Mateus, A.; Figueiras, J.; Martins, I.; Rodrigues, P.C.; Pinto, F. Relative Abundance and Compositional Variation of Silicates, Oxides and Phosphates in the W-Sn-Rich Lodes of the Panasqueira Mine (Portugal): Implications for the Ore-Forming Process. *Minerals* **2020**, *10*, 551. [[CrossRef](#)]
49. Iglesias, M.; Ribeiro, A. Zonas de cisaillement ductile dans l’arc Ibero-Armorican. *Serv. Geol. Port.* **1981**, *67*, 85–87.
50. González Clavijo, E.; Díez Balda, M.A.; Álvarez, F. Structural study of a semiductile strike-slip system in the Central Iberian Zone (Variscan Fold Belt, Spain): Structural controls on gold deposits. *Geol. Rund.* **1993**, *82*, 448–460. [[CrossRef](#)]
51. Pereira, E.; Ribeiro, A.; Meireles, C. Cisalhamentos hercínicos e controlo de mineralizações de Sn-W, Au e U na zona centro-Ibérica em Portugal. *Cuad. Lab. Xeol. Laxe Coruña* **1993**, *18*, 89–119.
52. Valle Aguado, B.; Martínez Catalán, J.R.; Azevedo, M.R. Structure of the western termination of the Juzbado-Penalva do Castelo Shear Zone (Western Iberian Massif). In *Variscan-Appalachian Dynamics: The Building of the Upper Paleozoic basement*; Program and Abstracts; Basement Tectonics: A Coruña, Spain, 2000; Volume 15, pp. 287–291.
53. Gutiérrez-Alonso, G.; Collins, A.S.; Fernández-Suárez, J.; Pastor-Galán, D.; González-Clavijo, E.; Jourdan, F.; Weil, A.B.; Johnston, S.T. Dating of lithospheric buckling:  $40\text{Ar}/39\text{Ar}$  ages of syn-orocline strike-slip shear zones in northwestern Iberia. *Tectonophysics* **2015**, *643*, 44–54. [[CrossRef](#)]
54. Pastor-Galán, D.; Dias da Silva, Í.; Groenewegen, T.; Krijgsman, W. Tangled up in folds: Tectonic significance of superimposed folding at the core of the Central Iberian curve (West Iberia). *Int. Geol. Rev.* **2019**, *61*, 240–255. [[CrossRef](#)]
55. Iglésias, M.; Choukroune, P. Shear zones in the Iberian Arc. *J. Struct. Geol.* **1980**, *2*, 63–68.
56. Ferreira, N.; Iglesias, M.; Noronha, F.; Pereira, E.; Ribeiro, A.; Ribeiro, M.L. Granitoides da Zona Centro Ibérica e seu enquadramento geodinâmico. In *Geologia de Los Granitoides y Rocas Asociadas del Macizo Hespérico Libro Homenaje a LC Garcia de Figuerola*; Bea, F., Carnicero, E., Gonzalo, J.C., Plaza, M.L., Rodríguez, M.D., Eds.; Rueda: Madrid, Spain, 1987; pp. 37–53.
57. Dias, G.T.; Leterrier, J.; Mendes, A.; Simões, P.P.; Bertrand, J.M. U-Pb zircon and monazite geochronology of post-collisional Hercynian granitoids from the Central Iberian Zone (Northern Portugal). *Lithos* **1998**, *45*, 349–369. [[CrossRef](#)]
58. Dias, G.; Simões, P.; Ferreira, N.; Leterrier, J. Mantle and crustal sources in the genesis of late-Hercynian granitoids (NW Portugal): Geochemical and Sr-Nd isotopic constraints. *Gond. Res.* **2002**, *5*, 287–305. [[CrossRef](#)]
59. Almeida, A.; Martins, H.; Noronha, F. Hercynian acid magmatism and related mineralisations in Northern Portugal. *Gond. Res.* **2002**, *5*, 423–434. [[CrossRef](#)]
60. Valle Aguado, B.; Azevedo, M.R.; Schaltegger, U.; Martínez-Catalán, J.R.; Nolan, J. U/Pb zircon and monazite geochronology of Variscan magmatism related to synconvergence extension in Central Northern Portugal. *Lithos* **2005**, *82*, 169–184. [[CrossRef](#)]
61. Martins, H.; Sant’Ovaia, H.; Noronha, F. Genesis and emplacement of felsic Variscan plutons within a deep crustal lineation, the Penacova-Régua-Verín fault: An integrated geophysics and geochemical study (NW Iberian Peninsula). *Lithos* **2009**, *111*, 142–155. [[CrossRef](#)]
62. Martins, H.; Sant’Ovaia, H.; Abreu, J.; Oliveira, M.; Noronha, F. Emplacement of the Lavadores granite (NW Portugal): U/Pb and AMS results. *Comptes Rendus Geosci.* **2011**, *343*, 387–396. [[CrossRef](#)]
63. Marques, F.O.; Mateus, A.; Tassinari, C.C. The Late-Variscan fault network in central-northern Portugal (NW Iberia): A re-evaluation. *Tectonophysics* **2002**, *359*, 255–270. [[CrossRef](#)]
64. Lagarde, J.L.; Capdevila, R.; Fourcade, S. Granites et collision continentale: L’exemple des granitoides carboniferes dans la chaine hercynienne ouesteuropéenne. *Bull. Soc. Géol.* **1992**, *163*, 597–610.
65. Escuder Viruete, J. Hornblende-bearing leucosome development during syn-orogenic crustal extension in the Tormes Gneiss Dome, NW Iberian Massif, Spain. *Lithos* **1999**, *46*, 751–772. [[CrossRef](#)]
66. López-Plaza, M.; Peinado, M.; López-Moro, F.J.; Rodríguez Alonso, M.D.; Carnicero, A.; Franco, P.; Gonzalo, J.C. Contrasting mantle sources and processes involved in a peri-Gondwanan terrane: A case study of pre-Variscan mafic intrusives from the autochthon of the Central Iberian Zone. *Geol. Soc. Am.-Spec. Pap.* **2007**, *423*, 297–313.
67. Fernández-Suárez, J.; Gutiérrez-Alonso, G.; Johnston, S.T.; Jeffries, T.E.; Pastor-Galán, D.; Jenner, G.A.; Murphy, J.B. Iberian late-Variscan granitoids: Some considerations on crustal sources and the significance of “mantle extraction ages”. *Lithos* **2011**, *123*, 121–132. [[CrossRef](#)]
68. López-Moro, F.J.; López-Plaza, M.; Gutiérrez-Alonso, G.; Fernández-Suárez, J.; López-Carmona, A.; Hofmann, M.; Romer, R.L. Crustal melting and recycling: Geochronology and sources of Variscan syn-kinematic anatexitic granitoids of the Tormes Dome (Central Iberian Zone). A U–Pb LA-ICP-MS study. *Int. J. Earth Sci.* **2017**, *107*, 985–1004. [[CrossRef](#)]

69. Arthaud, F.; Matte, P. Les décrochements Tardi-Hercyniens du Sud-ouest de l'Europe. Géometrie et essai de reconstitution des conditions de la déformation. *Tectonophysics* **1975**, *25*, 139–171. [[CrossRef](#)]
70. Sousa, M. Considerações sobre a estratigrafia do Complexo Xisto-Grauváquico (CXG) e a sua relação com o Paleozóico Inferior. *Quad. Geol. Ibérica* **1984**, *9*, 9–36.
71. Pereira, E. Estudo Geológico-Estrutural da Região de Celorico de Basto e a Sua Interpretação Geodinâmica. Ph.D. Thesis, University of Lisbon, Lisbon, Portugal, 1987; p. 274.
72. Sousa, M.; Sequeira, A. Carta Geológica de Portugal à escala 1/50.000, Folha 10-D–Alijó. *Serv. Geol. Port.* **1987**, *50*.
73. Meireles, C. New data on the lithostratigraphy of beiras Group (Schist Greywacke complex) in the region of Góis-Arganil-Pampilhosa da Serra (Central Portugal). *Cad. Lab. Xeolóxico Laxe* **2013**, *37*, 105–124. [[CrossRef](#)]
74. Silva, A. A Litostratigrafia e Estrutura do Supergrupo Dúrico-Beirão (Complexo Xisto-Grauváquico), em Portugal, e sua correlação com as correspondentes sucessões em Espanha. *Bolet. Minas* **2013**, *48*, 97–142.
75. San José, M.A.; Pieren, A.P.; García-Hidalgo, J.F.; Vilas, L.; Herranz, P.; Pelaez, J.R.; Perejon, A. Ante-Ordovician Stratigraphy. In *Pre-Mesozoic Geology of Iberia*; Dallmeyer, R.D., Martínez García, E., Eds.; Springer: Berlin, Germany, 1990; pp. 147–159.
76. Valladares, M.I.; Barba, P.; Ugidos, J.M.; Colmenero, J.R.; Armenteros, I. Upper Neoproterozoic–Lower Cambrian sedimentary successions in the Central Iberian Zone (Spain): Sequence stratigraphy, petrology and chemostratigraphy. Implications for other European zones. *Int. J. Earth Sci.* **2000**, *89*, 2–20. [[CrossRef](#)]
77. Ugidos, J.M.; Barba, P.; Valladares, M.I. Chapter Four—Review of the Upper Ediacaran-Lower Cambrian detrital series in Central and North Iberia: NE Africa as possible source area. In *Stratigraphy & Timescales*; Montenari, M., Ed.; Academic Press: Cambridge, MA, USA, 2020; Volume 5, pp. 147–268.
78. Castro, A.; Patiño Douce, A.E.; Corretgé, L.G.; De La Rosa, J.D.; El-Biad, M.; El-Hmidi, H. Origin of peraluminous granites and granodiorites, Iberian massif, Spain: An experimental test of granite petrogenesis. *Contrib. Mineral. Petrol.* **1999**, *135*, 255–276. [[CrossRef](#)]
79. Villaseca, C.; Downes, H.; Pin, C.; Barbero, L. Nature and Composition of the Lower Continental Crust in Central Spain and the Granulite-Granite Linkage: Inferences from Granulitic Xenoliths. *J. Petrol.* **1999**, *40*, 1465–1496. [[CrossRef](#)]
80. Ribeiro, M.; Castro, A.; Almeida, A.; González Menéndez, L.; Jesus, A.; Lains, J.A.; Lopes, J.C.; Martins, H.C.B.; Mata, J.; Mateus, A.; et al. Variscan Magmatism. In *The Geology of Iberia: A Geodynamic Approach, Volume 2, The Variscan Cycle*; Regional Geology Reviews; Springer: Gewerbestrasse, Switzerland, 2019; Volume 1, pp. 497–526.
81. Pinto, M.S.; Casquet, C.; Ibarrola, E.; Corretgé, L.S.; Ferreira, M.P. Síntese geocronológica dos granitóides do Maciço Hespérico. In *Geología de los Granitoides y Rocas Asociadas del Macizo Hespérico Libro Homenaje a L.C. Garcia de Figuerola*; Bea, F., Carnicero, E., Gonzalo, J.C., López Plaza, M., Rodríguez, M.D., Eds.; Rueda: Madrid, Spain, 1987; pp. 69–86.
82. Dias, G.T. Fontes de granitóides hercínicos da Zona Centro-Ibérica (Norte de Portugal): Evidências isotópicas (Sr, Nd). In *Geoquímica e Petrogênese de Rochas Granitoides*; Neiva, A.M.R., Ed.; Academia das Ciências de Lisboa: Lisboa, Portugal, 2001; pp. 21–43.
83. Azevedo, M.; Aguado, B. Origem e instalação de granitóides variscos na Zona Centro Ibérica. In *Geologia de Portugal no contexto da Ibéria*; Dias, R., Araújo, A., Terrinha, P., Kulberg, C., Eds.; University Évora: Évora, Portugal, 2006; pp. 107–121.
84. Mateus, A.; Noronha, F. Sistemas mineralizantes epigenéticos na Zona Centro-Ibérica; expressão da estruturação orogénica Meso-a Tardi-Varisca. In *Ciências Geológicas: Ensino e Investigação e sua História*; Coteló Neiva, J.M., Ribeiro, A., Mendes Victor, L., Noronha, F., Ramalho, M., Eds.; Associação Portuguesa de Geólogos and Sociedade Geológica de Portugal, Lisboa: Lisbon, Portugal, 2010; Volume II, pp. 47–61.
85. Inverno, C.; Ribeiro, M.L. Fracturação e cortejo filoniano nas Minas da Argemela (Fundão). *Comun. Serv. Geol. Port.* **1980**, *66*, 185–193.
86. Ribeiro, A.; Pereira, E. Controlos paleogeográficos, petrológicos e estruturais na génese dos jazigos portugueses de estanho e volfrâmio. *Geonovas* **1982**, *1*, 23–31.
87. Derré, C.; Lécolle, M.; Roger, G.; Carvalho, J. Tectonics, magmatism, hydrothermalism and sets of flat joints locally filled by Sn-W aplite-pegmatite and quartz veins; southeastern border of the Serra da Estrela granitic massif (Beira Baixa, Portugal). *Ore Geol. Rev.* **1986**, *1*, 43–56. [[CrossRef](#)]
88. Ribeiro, M.L. Modelos de implantação dos granitos variscos portugueses. In *Geoquímica e Petrogênese de Rochas Granitoides*; Neiva, A.M.R., Ed.; Academia das Ciências de Lisboa: Lisboa, Portugal, 2001; pp. 33–52.
89. Cathelineau, M.; Boiron, M.C.; Marignac, C.; Dour, M.; Dejean, M.; Carocci, E.; Truche, L.; Pinto, F. High pressure and temperatures during the early stages of tungsten deposition at Panasqueira revealed by fluid inclusions in topaz. *Ore Geol. Rev.* **2020**, *126*, 103741. [[CrossRef](#)]
90. Noronha, F. Estudo Metalogénico da Área Tunstífera da Borralha. Ph.D. Thesis, University Porto, Porto, Portugal, 1983; p. 413.
91. Noronha, F.; Vindel, E.; López, J.A.; Dória, A.; Garcia, E.; Boiron, M.-C.; Cathelineau, M. Fluids related to tungsten ore deposits in Northern Portugal and Spanish Central System: A comparative study. *Rev. Soc. Geol. España* **1999**, *12*, 397–403.
92. Conde, L.; Pereira, V.; Ribeiro, A.; Thadeu, D. Jazigos Hipogénicos de Estanho e volfrâmio. In *I Congresso Hispano-Luso-Americano de Geologia Económica*; Direção Geral de Minas e Serviços Geológicos: Lisboa, Portugal, 1979; p. 81.
93. Thadeu, D. Características da mineralização hipogénica estano-volframítica portuguesa. *Bol. Ord. Eng.* **1965**, *10*, 61–81.
94. Clark, A.H. Preliminary of the temperatures and confining pressures of granite emplacement and mineralization, Panasqueira, Portugal. *Trans. Inst. Min. Metall.* **1964**, *73*, 813–824.

95. Portugal Ferreira, M.; Costa, V.; Regêncio Macedo, C.A.; Gama Pereira, L. Datações K-Ar em biotite das rochas granitóides da Cova da Beira (Portugal Central). *Mem. Not. Publ. Mus. Lab. Mineral. Geol.* **1977**, *84*, 39–48.
96. Kelly, W.C.; Reye, R.O. Geologic, fluid inclusion, and stable isotope studies of the tin-tungsten deposits of Panasqueira, Portugal. *Econ. Geol.* **1979**, *74*, 1721–1882. [[CrossRef](#)]
97. Bussink, R.W. Geochemistry of the Panasqueira tungsten-tin deposit, Portugal. *Geol. Ultraiect.* **1984**, *33*, 1–159.
98. Priem, D.; Tex, T. Tracing crustal evolution in the NW Iberian Peninsula through the Rb-Sr and U-Pb systematics of Paleozoic granitoids: A review. *Phys. Earth Planet. Inter.* **1984**, *35*, 121–130. [[CrossRef](#)]
99. Pereira, A.; Pereira, L.; Macedo, C. Os plutonitos da zebreira (Castelo Branco): Idade e enquadramento estrutural. *Mem. Not. Publ. Mus. Lab. Mineral. Geol.* **1986**, *101*, 21–31.
100. Antunes, I.M.; Neiva, A.M.; Silva, M.M.; Corfu, F. Geochemistry of S-type granitic rocks from the reversely zoned Castelo Branco pluton (central Portugal). *Lithos* **2008**, *103*, 445–465. [[CrossRef](#)]
101. Antunes, I.M.; Neiva, A.M.; Silva, M.M.; Corfu, F. The genesis of I- and S-type granitoid rocks of the Early Ordovician Oledo pluton, Central Iberian Zone (central Portugal). *Lithos* **2009**, *111*, 168–185. [[CrossRef](#)]
102. Antunes, I.M.; Neiva, A.M.; Corfu, F. New emplacement age to the Fundão pluton (central Portugal): U-Pb isotopic data. In Proceedings of the European Mineralogical Conference, Frankfurt, Germany, 2–6 September 2012.
103. Antunes, I.M.; Neiva, A.M.; Ramos, J.M.; Silva, P.B.; Silva, M.M.; Corfu, F. Petrogenetic links between lepidolite-subtype aplite-pegmatite, aplite veins and associated granites at Segura (central Portugal). *Geochemistry* **2013**, *73*, 323–341. [[CrossRef](#)]
104. Antunes, I.M. Características geoquímicas e geocronológicas do plutão de Fundão—Implicações geotectónicas. In Proceedings of the XII Congresso Ibérico de Geoquímica, Évora, Portugal, 22–26 September 2019; pp. 133–136.
105. Martins Peres, A.; Caraça Valente, A.J.; Lucas Gonçalves, J. Carta Geológica de Portugal à escala 1/50.000, Folha 21-B—Quadrasais. *Serv. Geol. Port.* **1960**.
106. Avila Martins, J.; Cândido de Medeiros, A.; Peres, A.; Pilar, L.; Pinto Mesquita, L. Carta Geológica de Portugal à escala 1/50.000, Folha 21-A- Sabugal. *Serv. Geol. Port.* **1964**.
107. Ribeiro, O.; Ribeiro Ferreira, C. Carta Geológica de Portugal à escala 1/50.000, Folha 24-D—Castelo Branco. *Serv. Geol. Port.* **1966**.
108. Perdígão, J.C.; Moreira, P.A. Carta Geológica de Portugal à escala 1/50.000, Folha 21-D—Vale Feitoso. *Serv. Geol. Port.* **1975**.
109. Teixeira, C.; de Carvalho, H.; Paula Santos, J. Carta Geológica de Portugal à escala 1/50.000, Folha 20-B—Covilhã. *Serv. Geol. Port.* **1975**.
110. Oliveira, J.T.; Pereira, E.; Ramalho, M.; Antunes, M.T.; Monteiro, J.H. Carta Geológica de Portugal à escala 1/500.000. *Serv. Geol. Port.* **1992**.
111. Sequeira, A.; Proença Cunha, P.; Ribeiro, M. Carta Geológica de Portugal à escala 1/50.000, Folha 25-B—Salvaterra do Extremo. *Inst. Geol. Min.* **1999**.
112. Romão, J.; Ferreira da Silva, A.; Proença Cunha, P.; Pereira, A. Carta Geológica de Portugal à escala 1/50.000, Folhas 25-C, 25-D e 29-A—Rosmaninhal, Segura e Retorta. *Lab. Geol. Min.* **2010**.
113. Gonçalves, A.; Sant’Ovaia, H.; Noronha, F. Geochemical Signature and Magnetic Fabric of Capinha Massif (Fundão, Central Portugal): Genesis, Emplacement and Relation with W–Sn Mineralizations. *Minerals* **2020**, *10*, 557. [[CrossRef](#)]
114. Neiva, A.M.; Costa Campos, T. Genesis of the zoned granitic pluton of Penamacor-Monsanto, Central Portugal. *Mem. Not. Publ. Mus. Lab. Mineral. Geol.* **1992**, *114*, 51–68.
115. Ribeiro da Costa, I.; Antunes, I.M.; Mourão, C.; Recio, C.; Guimarães, F.; Ramos, J.F.; Barriga, F.J.A.S. Contact metamorphism associated to the Penamacor-Monsanto granitic intrusion (Central Portugal): Geochemical, isotopic and mineralogical features. *J. Iber. Geol.* **2018**, *44*, 335–353. [[CrossRef](#)]
116. Michaud, J.A.S.; Pichavant, M. Magmatic fractionation and the magmatic-hydrothermal transition in rare metal granites: Evidence from Argemela (Central Portugal). *Geochim. Cosmochim. Acta* **2020**, *289*, 130–157. [[CrossRef](#)]
117. Marignac, C.; Cuney, M.; Cathelineau, M.; Lecomte, A.; Carocci, E.; Pinto, F. The Panasqueira Rare Metal Granite Suites and Their Involvement in the Genesis of the World-Class Panasqueira W–Sn–Cu Vein Deposit: A Petrographic, Mineralogical, and Geochemical Study. *Minerals* **2020**, *10*, 562. [[CrossRef](#)]
118. Debon, F.; Lefort, P. A cationic classification of common plutonic rocks and their magmatic associations: Principles, method, applications. *Bul. Min.* **1988**, *111*, 493–510. [[CrossRef](#)]
119. Shand, S.J. *Eruptive Rocks. Their Genesis Composition. Classification, and Their Relation to Ore-Deposits with a Chapter on Meteorite*; John Wiley & Sons, Ltd.: Hoboken, NJ, USA, 1943.
120. Frost, B.R.; Barnes, C.G.; Collins, W.J.; Argulus, R.J.; Ellis, D.J.; Frost, C.D. A geochemical classification for granitic rocks. *J. Petrol.* **2001**, *42*, 2033–2048. [[CrossRef](#)]
121. Frost, B.R.; Frost, C.D. A geochemical classification for feldspathic igneous rocks. *J. Petrol.* **2008**, *49*, 1955–1969. [[CrossRef](#)]
122. El Bouseily, A.; El Sokkary, A. The relation between Rb, Ba, and Sr in granitic rocks. *Geochem. Geol.* **1975**, *16*, 207–219. [[CrossRef](#)]
123. Pearce, J.A.; Harris, N.B.W.; Tindle, A.G. Trace element discrimination diagrams for the tectonic interpretation of granitic rocks. *J. Petrol.* **1984**, *25*, 956–983. [[CrossRef](#)]
124. Cuney, M. Felsic magmatism and uranium deposits. *Bull. Soc. Géol. France* **2014**, *185*, 75–92. [[CrossRef](#)]
125. Rudnick, R.L.; Gao, S. Composition of the continental crust. *Treat. Geoch.* **2014**, *4*, 1–51.
126. McDonough, W.F.; Sun, S.S. The composition of the Earth. *Chem. Geol.* **1995**, *120*, 223–253. [[CrossRef](#)]

127. Yuan, S.D.; Williams-Jones, A.E.; Mao, J.W.; Zhao, P.L.; Yan, C.; Zhang, D.L. The origin of the Zhangjianlong tungsten deposit, South China: Implications for W-Sn mineralization in large granite batholiths. *Econ. Geol.* **2018**, *113*, 1193–1208. [[CrossRef](#)]
128. Castro, A.; Pereira, M.F.; Rodríguez, C.; Fernández, C.; de la Rosa, J.D. Atypical peri-Gondwanan granodiorite-tonalite magmatism from Southern Iberia. Origin of magmas and implications. *Lithos* **2020**, *372–373*, 1–14. [[CrossRef](#)]
129. López-Moro, F.J.; Polonio, F.G.; González, T.L.; Contreras, J.L.S.; Fernández, A.F.; Benito, M.C.M. Ta and Sn concentration by muscovite fractionation and degassing in a lens-like granite body: The case study of the Penouta rare-metal albite granite (NW Spain). *Ore Geol. Rev.* **2017**, *82*, 10–30. [[CrossRef](#)]
130. Roda-Robles, E.; Villaseca, C.; Pesquera, A.; Gil-Crespo, P.P.; Vieira, R.; Lima, A.; Garate-Olave, I. Petrogenetic relationships between Variscan granitoids and Li-(F-P)-rich aplite-pegmatites in the Central Iberian Zone: Geological and geochemical constraints and implications for other regions from the European Variscides. *Ore Geol. Rev.* **2018**, *95*, 408–430. [[CrossRef](#)]
131. Audétat, A.; Günther, D.; Heinrich, C.A. Magmatic-hydrothermal evolution in a fractionating granite: A microchemical study of the Sn-WF-mineralized Mole Granite (Australia). *Geoch. Cosm Acta* **2000**, *64*, 3373–3393. [[CrossRef](#)]
132. Simons, B.; Andersen, J.C.; Shail, R.K.; Jenner, F.E. Fractionation of Li, Be, Ga, Nb, Ta, In, Sn, Sb, W and Bi in the peraluminous early permian Variscan granites of the Cornubian Batholith: Precursor processes to magmatic-hydrothermal mineralisation. *Lithos* **2017**, *278*, 491–512. [[CrossRef](#)]
133. Michaud, J.A.S.; Gumiaux, C.; Pichavant, M.; Gloaguen, E.; Marcoux, E. From magmatic to hydrothermal Sn-Li-(Nb-Ta-W) mineralization: The Argemela area (central Portugal). *Ore Geol. Rev.* **2020**, *116*, 103215. [[CrossRef](#)]
134. Zhao, P.L.; Zajacz, Z.; Tsay, A.; Yuan, S.D. Magmatic-hydrothermal tin deposits form in response to efficient tin extraction upon magma degassing. *Geochim. Cosmoch. Acta* **2022**, *316*, 331–346. [[CrossRef](#)]